Please cite this article in press as: Georgiou et al., AAV9-mediated *SH3TC2* gene replacement therapy targeted to Schwann cells for the treatment of CMT4C, Molecular Therapy (2023), https://doi.org/10.1016/j.ymthe.2023.08.020

Molecular Therapy
Original Article

AAV9-mediated *SH3TC2* gene replacement therapy targeted to Schwann cells for the treatment of CMT4C

Elena Georgiou,[1] Alexia Kagiava,[1] Irene Sargiannidou,[1] Natasa Schiza,[1] Marina Stavrou,[1] Jan Richter,[2] Christina Tryfonos,[2] Amanda Heslegrave,[3,4] Henrik Zetterberg,[3,4,5,6,7,8] Christina Christodoulou,[2] and Kleopas A. Kleopa[1,9]

[1]Neuroscience Department, The Cyprus Institute of Neurology and Genetics, Nicosia, Cyprus; [2]Molecular Virology Department, The Cyprus Institute of Neurology and Genetics, Nicosia, Cyprus; [3]Department of Neurodegenerative Disease, UCL Institute of Neurology, London, UK; [4]UK Dementia Research Institute at UCL, London, UK; [5]Department of Psychiatry and Neurochemistry, Institute of Neuroscience and Physiology, the Sahlgrenska Academy at the University of Gothenburg, Mölndal, Sweden; [6]Clinical Neurochemistry Laboratory, Sahlgrenska University Hospital, Mölndal, Sweden; [7]Hong Kong Center for Neurodegenerative Diseases, Clear Water Bay, Hong Kong, China; [8]Wisconsin Alzheimer's Disease Research Center, University of Wisconsin School of Medicine and Public Health, University of Wisconsin-Madison, Madison, WI, USA; [9]Center for Neuromuscular Disorders, The Cyprus Institute of Neurology and Genetics, Nicosia, Cyprus

Type 4C Charcot-Marie-Tooth (CMT4C) demyelinating neuropathy is caused by autosomal recessive *SH3TC2* gene mutations. *SH3TC2* is highly expressed in myelinating Schwann cells. CMT4C is a childhood-onset progressive disease without effective treatment. Here, we generated a gene therapy for CMT4C mediated by an adeno-associated viral 9 vector (AAV9) to deliver the human *SH3TC2* gene in the *Sh3tc2*$^{-/-}$ mouse model of CMT4C. We used a minimal fragment of the myelin protein zero (*Mpz)* promoter (mini*Mpz*), which was cloned and validated to achieve Schwann cell-targeted expression of *SH3TC2*. Following the demonstration of AAV9-mini*Mpz.SH3TC2myc* vector efficacy to re-establish SH3TC2 expression in the peripheral nervous system, we performed an early as well as a delayed treatment trial in *Sh3tc2*$^{-/-}$ mice. We demonstrate both after early as well as following late treatment improvements in multiple motor performance tests and nerve conduction velocities. Moreover, treatment led to normalization of the organization of the nodes of Ranvier, which is typically deficient in CMT4C patients and *Sh3tc2*$^{-/-}$ mice, along with reduced ratios of demyelinated fibers, increased myelin thickness and reduced g-ratios at both time points of intervention. Taken together, our results provide a proof of concept for an effective and potentially translatable gene replacement therapy for CMT4C treatment.

INTRODUCTION

Type 4C Charcot-Marie-Tooth (CMT4C) disease has emerged as the most common type among the rare autosomal recessive (AR) demyelinating neuropathies collectively known as CMT4.[1,2] Among undiagnosed Italian CMT4 patients, *SH3TC2* mutation frequency reached 30%,[3] while among 612 index cases with different CMT types (AD, X, AR), *SH3TC2* mutations were found in 9.9%, and in 29.3% of the AR cases.[4] The disease typically appears during the first 10 years of life (range 1–14 years) with manifestations including pes cavus deformities, distal muscle weakness, areflexia, and sensory loss, as well as progressive scoliosis.[5–8] Involvement of the cranial nerves is common presenting with hearing impairment, slow pupillary light reflexes, and tongue fasciculations.[9–11] Electrophysiological studies in CMT4C patients are consistent with a demyelinating pathology, showing median motor nerve conduction velocity (MNCV) of approximately 22.6 m/s. Biopsied CMT4C nerves reveal excessive basal membranes surrounding thinly myelinated or demyelinated axons, and large extensions of Schwann cell cytoplasm, while there is also a characteristic elongation of the node of Ranvier.[5,6,12,13]

SH3TC2 gene mutations described to date include mostly premature stop codons and single amino acid (aa) substitutions.[12] They may be more common among certain ethnic groups[14] likely due to founder effects.[9] The full transcript of *SH3TC2* cDNA measures 3,864 bp encoding a 1,288-aa protein that includes 2 Src homology 3 (SH3) and 10 tetratricopeptide repeat domains, and differs from any other functionally characterized protein. This structure indicates a scaffolding function.[12] The *SH3TC2* gene is well preserved between vertebrate species, while non-vertebrate orthologs have not been discovered. The SH3TC2 protein is a component of the intracellular pathway of early and late endosomes with clathrin-coated vesicles, near the *trans*-Golgi network and cell membrane. CMT4C mutations change this cellular expression of SH3TC2.[15]

Recapitulating the major aspects of human disease, a CMT4C mouse model has been generated by deleting the *Sh3tc2* gene. *Sh3tc2*$^{-/-}$

Received 14 February 2023; accepted 25 August 2023;
https://doi.org/10.1016/j.ymthe.2023.08.020.

Correspondence: Kleopas A. Kleopa, MD, FAAN, Neuroscience Department, The Cyprus Institute of Neurology and Genetics, Nicosia, Cyprus.
E-mail: kleopa@cing.ac.cy

Please cite this article in press as: Georgiou et al., AAV9-mediated *SH3TC2* gene replacement therapy targeted to Schwann cells for the treatment of CMT4C, Molecular Therapy (2023), https://doi.org/10.1016/j.ymthe.2023.08.020

mice are characterized by slow motor and sensory nerve conduction velocities, as well as progressive hypo- and demyelination from age 2 to 12 months.[13,16] Sh3tc2 is highly expressed in murine Schwann cells with localization to the cell membrane and endocytic recycling vesicles, indicating a functional role in myelin formation and in axon-glial interactions.[17] As also observed in biopsied nerves from CMT4C patients, myelinated fibers from *Sh3tc2*$^{-/-}$ mice present a characteristic widening of the node of Ranvier, indicating an important role of SH3TC2 in the organization of the nodal region.[13] Thus, the *Sh3tc2*$^{-/-}$ mouse provides an appropriate model to test potential CMT4C treatments.

The effectiveness of *SH3TC2* gene replacement therapy for CMT4C was previously shown using an intrathecally injected lentiviral vector expressing *SH3TC2* cDNA along with myc tag driven by the full-length 1.2-kb rat myelin protein zero (*Mpz*) promoter.[18] Nevertheless, lentiviral-mediated expression levels in Schwann cells led to a partial phenotype rescue. To achieve a stronger therapeutic effect, better vector biodistribution and gene expression rates are needed. Therefore, we tested as an alternative an adeno-associated viral (AAV) vector[19–23] that could provide higher expression levels, while its episomal persistence without integration into the host genome increases the safety of *in vivo* delivery.[24,25] We chose the AAV9 serotype already used in other clinical application including for the treatment of spinal muscular atrophy (SMA) after extensive safety evaluation in pre-clinical[26,27] and in phase 1 (NCT02122952) and phase 3 (NCT03461289) clinical trials. AAV9 has shown effective Schwann cell targeting in our previous applications for CMT1X[22] and CMT1A.[28] Here, we demonstrate that AAV9 provides Schwann cell-specific expression of *SH3TC2* driven by a minimal version of the *Mpz* promoter (mini*Mpz*) leading to significant functional and morphological improvements in the *Sh3tc2*$^{-/-}$ mouse when delivered at early as well as at late stages of the neuropathy. However, improvement in most outcome measures was modest and did not reach the level of age-matched wild-type (WT) animals.

RESULTS

Cloning and *in vivo* validation of a minimal *Mpz* promoter

To exploit the high potential of the AAV9-mediated gene therapy approach for clinical translation to treat CMT4C, we first had to overcome the limitation of smaller transgene capacity of AAV vectors. To facilitate an AAV-mediated *SH3TC2* coding sequence delivery, we used the 1.2-kb full-length rat *Mpz* promoter previously shown to drive Schwann cell-specific gene expression[29,30] for cloning a minimal *Mpz* promoter version to achieve targeted Schwann cell-specific expression while remaining within the carrying capacity of AAV vector. Since enhancer/ChIP-seq data indicate that essential functional regulatory elements (Egr2 and Sox10 binding sites) of the full-length *Mpz* promoter are located within 400 bp upstream of the start codon,[31] we PCR amplified the distal 410-bp sequence from the *Mpz* promoter. We further cloned this mini*Mpz* promoter into the AAV transfer plasmid along with downstream *EGFP* as a reporter gene, to produce the AAV9-mini*Mpz.EGFP* vector (Figure 1A).

The AAV9-mini*Mpz.EGFP* vector was delivered by lumbar intrathecal injection into 2-month-old WT mice. Vector biodistribution and EGFP expression were analyzed 5 weeks after injection. High vector genome copy numbers (VGCNs) were detected in DNA extracted from peripheral nervous system (PNS) tissues with a gradient from injection site toward the sciatic nerves, reaching 2.41 ± 0.31 in lumbar roots and 0.48 ± 0.33 in sciatic nerves (n = 5 mice; Figure 1B). Examination of fixed lumbar spinal root sections attached to the spinal cord, and of bilateral sciatic nerve sections and teased fibers revealed widespread expression of EGFP reporter gene in the perinuclear cytoplasm restricted to myelinating Schwann cells in PNS tissues of the injected mice, in contrast to non-injected controls (Figures 1C–1G). The percentage of EGFP-expressing cells reached an average of 56.93% ± 3.21% in anterior lumbar roots and 55.17% ± 6.88% in sciatic nerves (n = 5 mice; Figure 1H).

Immunostaining for EGFP combined with CNS cell markers was carried out in lumbar spinal cord sections to validate the cell specificity of the *Mpz* promoter. This analysis showed that EGFP expression was present in a very low percentages of oligodendrocytes (2.58% ± 0.96%) and neurons (1.92% ± 0.25%), while it was undetectable in astrocytes (Figure S1).

AAV9-mini*Mpz-SH3TC2myc* vector cloning and SH3TC2 expression in *Sh3tc2*$^{-/-}$ mice

The novel AAV9-mini*Mpz-SH3TC2myc* therapeutic construct was cloned by ligating the *SH3TC2myc* sequence[18] downstream of the mini*Mpz* promoter, while the woodchuck hepatitis virus post-transcriptional regulatory element (WPRE) and bovine growth hormone polyadenylation sequence (bGHpA) elements were replaced by a small synthetic poly(A) (Figure 2A). This expression cassette was successfully packaged into the AAV9 capsid with vector production achieving titers of 5×10^{12} vg/mL. A total of 2×10^{11} vg in a volume of 20 μL was delivered by lumbar intrathecal injection into 2-month-old *Sh3tc2*$^{-/-}$ mice (n = 5 mice). Vector biodistribution and expression was examined 5 weeks after injection. DNA extracted from spinal roots and sciatic nerves of injected mice showed high levels of vector biodistribution throughout the PNS with VGCNs reaching 2.41 ± 0.93 in spinal roots and 2.06 ± 1.34 for sciatic nerves (Figure 2B). Immunostaining for human SH3TC2 in lumbar spinal root sections, as well as in sciatic nerve sections and teased fibers confirmed the presence of virally expressed SH3TC2 in the perinuclear Schwann cell cytoplasm in all PNS tissues, in a characteristic perinuclear granular appearance, and occasionally along the entire length of the Schwann cell, while it was absent from tissues of non-injected *Sh3tc2*$^{-/-}$ mice stained as negative controls (Figures 2C–2G). Quantification of the percentage of SH3TC2-immunoreactive Schwann cells showed average expression rates of 54.67% ± 4.72% in spinal roots and 45.39% ± 3.39% in sciatic nerves (Figure 2H). Thus, we were able to achieve adequate therapeutic vector biodistribution and high SH3TC2 expression rates in Schwann cells.

Functional improvements following early treatment in the CMT4C model

After confirming the high expression efficiency of the novel therapeutic vector AAV9-mini*Mpz-SH3TC2myc*, we performed a

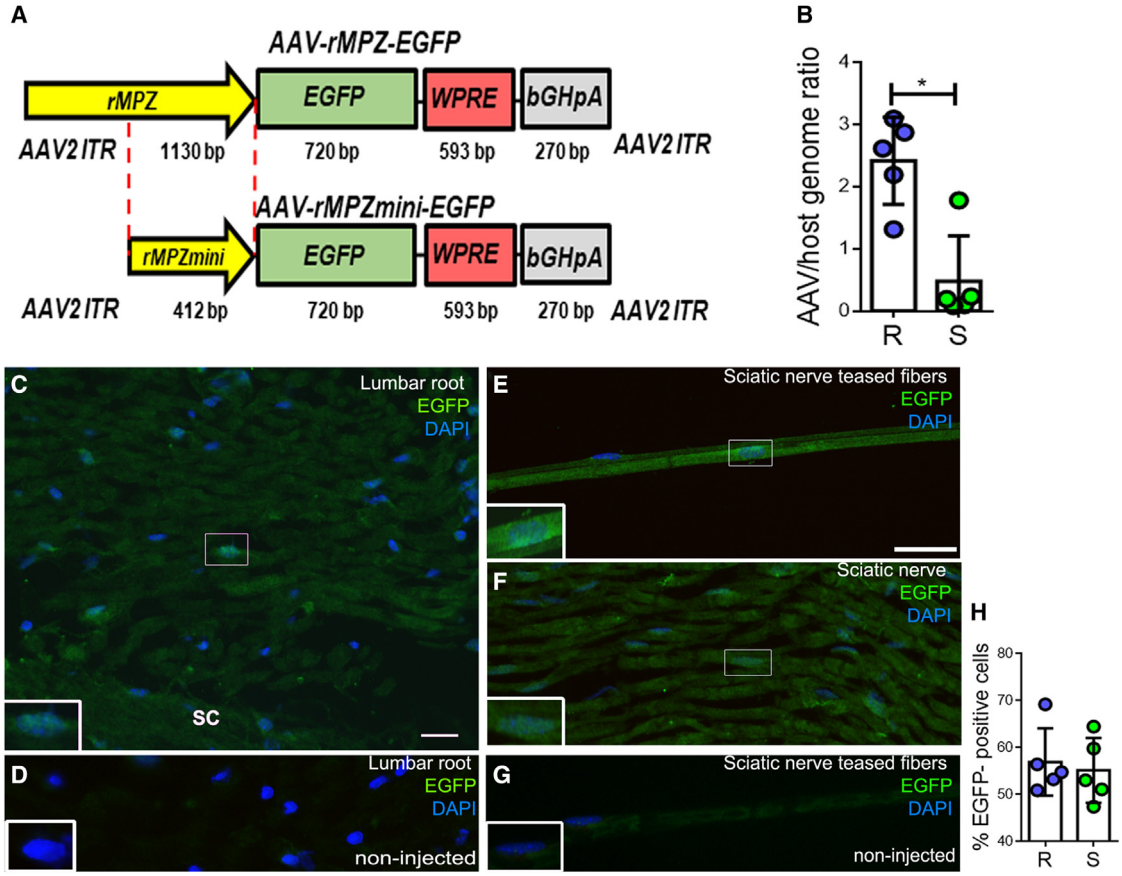

Figure 1. Cloning and validation of a minimal Mpz promoter

(A) Generation of the AAV9-mini*Mpz.EGFP* vector (mock vector driving reporter gene expression) through cloning of the distal 412 fragment of the full-length rat myelin protein zero (Mpz) promoter. (B) Biodistribution of the AAV9-mini*Mpz.EGFP* in PNS tissues including sciatic nerves (S) and lumbar roots (R) of WT mice 5 weeks following lumbar intrathecal injection (vector genome copy numbers represent the ratio of vector to host genome in each tissue). Expression of EGFP in Schwann cells in lumbar roots (C), sciatic nerve sections (F), and sciatic nerve teased fibers (E) following intrathecal injection of the AAV9-mini*Mpz.EGFP* vector. EGFP shows the characteristic perinuclear cytoplasmic immunoreactivity in most myelinating Schwann cells, while EGFP expression was absent from corresponding tissues of non-injected mice (D and G). (H) Quantification of expression rates (% EGFP-positive cells) in bilateral sciatic nerves and lumbar spinal roots from n = 5 injected mice showed an average of 56.93% expression rates in roots and 55.17% in sciatic nerves. Values represent mean ± SEM. Scale bars, 20 μm.

randomized, mock vector-controlled treatment trial at early (age 1 month) stages of neuropathy. The level of phenotypic rescue in treated animals was compared with mock-treated littermates (injected with the mock vector AAV-mini*Mpz-EGFP*) by motor-behavioral, electrophysiological, and morphological studies 2 months after treatment. For the early gene therapy trial, two groups (n = 20 per group) of *Sh3tc2*$^{-/-}$ mice and age-matched WT mice (n = 10–12 mice) were assessed by behavioral testing at age 1 and at 3 months (2 months after injection) and sacrificed afterward either for quantitative morphometric analysis (n = 10 per group) or for electrophysiological evaluation (n = 10 per treatment group and n = 5–6 mice for WT controls) (Figure 3A). VGCNs determined 8 weeks after injection reached 0.48 ± 0.1 in lumbar roots and 0.18 ± 0.05 in the sciatic nerves (n = 7; Figure 3B), while the percentage of SH3TC2-expressing cells reached an average of 58.95% ± 2.6% in anterior lumbar roots and 43.1% ± 4.7% in sciatic nerves (n = 4 mice; Figure 3C).

We have focused our behavioral analysis of treated and mock-treated animals on testing motor strength and coordination. Time course analysis of the rotarod tests showed improved motor performance in AAV9-mini*Mpz.SH3TC2myc*-treated *Sh3tc2*$^{-/-}$ mice approaching the performance of age-matched WT mice at lower but not at higher speed tested, whereas AAV9-mini*Mpz.EGFP*-treated *Sh3tc2*$^{-/-}$ mice showed deterioration over time (Figures 3D–3I). Foot grip strength in early-treatment groups at age 1 month, at baseline before starting treatment, detected no difference between them. At age 3 months (2 months post-injection) muscle strength improved in fully treated mice compared with the mock group and reached WT levels. Longitudinal comparison also demonstrated that the strength

Please cite this article in press as: Georgiou et al., AAV9-mediated *SH3TC2* gene replacement therapy targeted to Schwann cells for the treatment of CMT4C, Molecular Therapy (2023), https://doi.org/10.1016/j.ymthe.2023.08.020

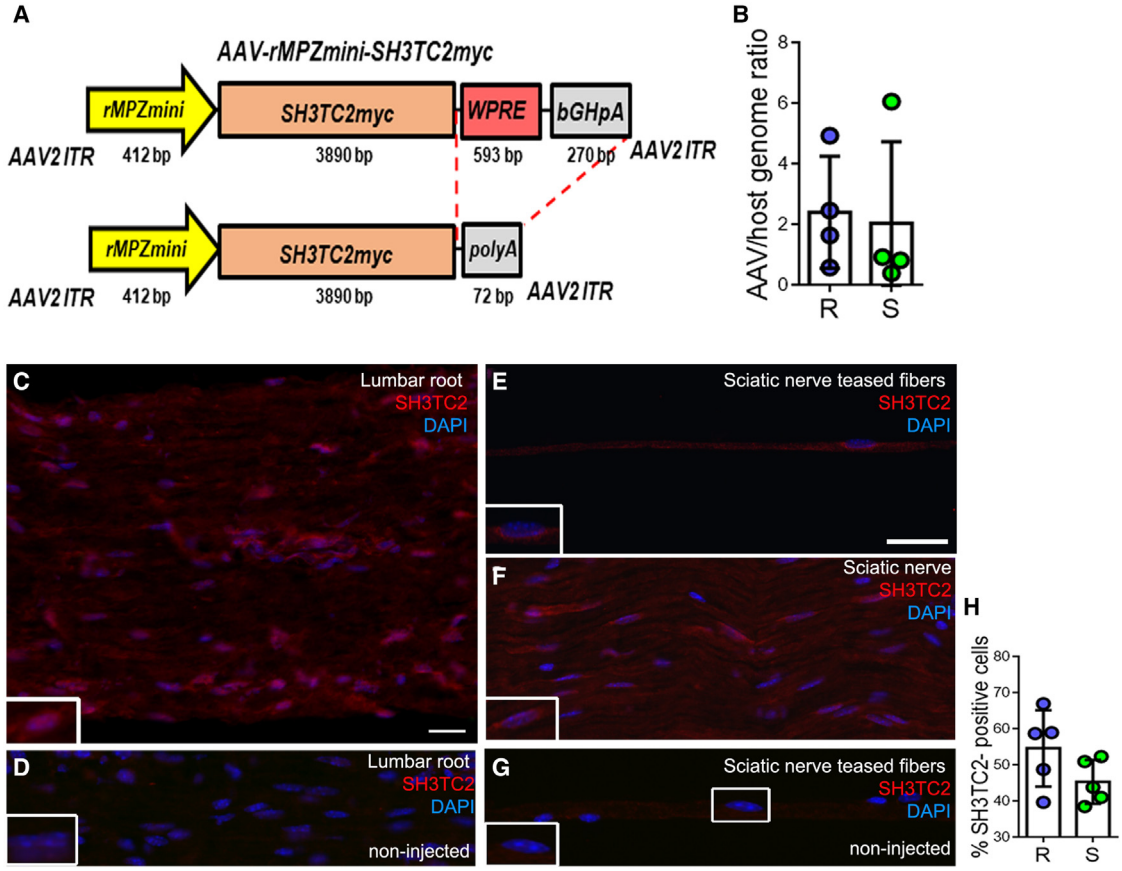

Figure 2. Cloning and expression of the therapeutic vector AAV9-mini*Mpz.SH3TC2myc*

(A) Cloning of the AAV9-mini*Mpz.SH3TC2myc* vector for expression of the human SH3TC2 gene under the control of mini*Mpz* promoter to treat CMT4C. To generate the size-optimized therapeutic vector plasmid the WPRE element has been removed and the bGHpA (270 bp) has been replaced by a minimal synthetic poly(A) (72 bp) to a final total size of 4,793 bp from ITR to ITR. (B) Biodistribution of novel AAV9-mini*Mpz-SH3TC2myc* therapeutic vector in sciatic nerves (S) and lumbar roots (R) of *Sh3tc2*$^{-/-}$ mice 5 weeks following lumbar intrathecal injection (vector genome copy numbers represent the ratio of vector to host genome in each tissue). Analysis of SH3TC2 expression in lumbar roots (C), sciatic nerve sections (F), and sciatic nerve teased fibers (E) following intrathecal injection of the AAV9-mini-*Mpz.SH3TC2myc* vector shows the characteristic granular perinuclear cytoplasmic immunoreactivity of SH3TC2 in the perinuclear cytoplasm of myelinating Schwann cells, while SH3TC2 expression is absent from the corresponding tissues of non-injected *Sh3tc2*$^{-/-}$ mice (D and G). (H) Quantification of expression rates (% SH3TC2-expressing cells) in bilateral sciatic nerves and lumbar spinal roots from n = 5 mice showed an average of 54.67% expression rates in roots and 45.4% in sciatic nerves. Values represent mean ± SEM. Scale bars, 20 μm.

produced by the hindlimbs improved with time in treated mice in contrast to mice treated with the mock vector (Figures 3J–3L).

Nerve conduction studies in 3-month-old mice (2 months after treatment) (Figures 3M and 3N) revealed significantly improved sciatic nerve MNCVs in AAV9-mini*Mpz.SH3TC2myc*-treated mice (29.41 ± 2.5 m/s) compared with the mock-treated group (23.78 ± 2.01 m/s), although not reaching those of age-matched WT animals (43.69 ± 0.48 m/s). There was also a trend for higher compound muscle action potential (CMAP) amplitude in AAV9-mini*Mpz.SH3TC2myc*-treated mice (2.29 ± 0.31 mV) compared with the mock group (1.97 ± 0.26 mV), but without reaching statistical significance and also remaining below WT levels (4.6 ± 1.88 mV). In addition, pre-onset treatment with AAV9-mini-*Mpz.SH3TC2myc* improved the hindlimb clasping phenotype characteristic of *Sh3tc2*$^{-/-}$ mice (Figures 3O and 3P).

Improved nodal morphology in early-treated CMT4C model

Given that nodal widening is already present in 1-month-old *Sh3tc2*$^{-/-}$ mice as well as in biopsied nerves from CMT4C patients,[13] we further evaluated nodal pathology to assess if gene replacement could improve this early onset pathological finding of CMT4C. Immunofluorescent staining of sciatic nerve teased fibers in 3-month-old mice (2 months after vector injection) for Nav1.6, a nodal marker, and for Caspr, a paranodal axonal protein, showed the typical nodal widening in nerve fibers from mock-treated *Sh3tc2*$^{-/-}$ mice, while nodal length was reduced in fully treated *Sh3tc2*$^{-/-}$ mice approaching that of WT animals (Figure 3Q).

Please cite this article in press as: Georgiou et al., AAV9-mediated *SH3TC2* gene replacement therapy targeted to Schwann cells for the treatment of CMT4C, Molecular Therapy (2023), https://doi.org/10.1016/j.ymthe.2023.08.020

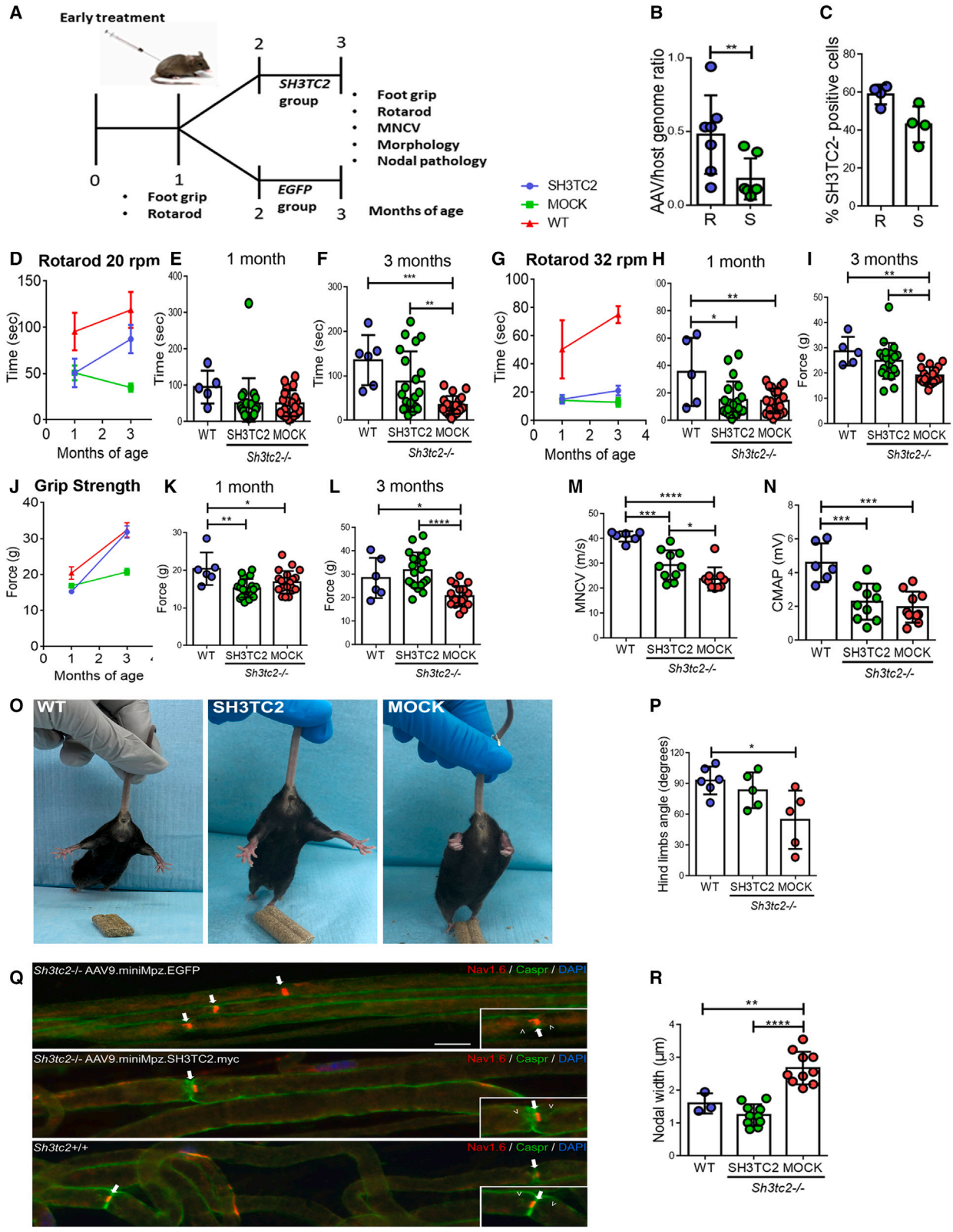

(legend on next page)

Please cite this article in press as: Georgiou et al., AAV9-mediated *SH3TC2* gene replacement therapy targeted to Schwann cells for the treatment of CMT4C, Molecular Therapy (2023), https://doi.org/10.1016/j.ymthe.2023.08.020

Quantification of 50 nodes per mouse from n = 10 *Sh3tc2*$^{-/-}$ mice per treatment group along with 50 nodes from n = 3 WT mice, confirmed a complete rescue of nodal length in treated animals (Figure 3R). Thus, even this early onset abnormality caused by the loss of SH3TC2 can be reversed following gene replacement.

Improved PNS myelination in early-treated CMT4C mice

Morphological examination was carried out in transverse toluidine-stained semithin sections of motor lumbar roots and mid-sciatic and femoral motor nerves of 3-month-old *Sh3tc2*$^{-/-}$ mice injected with the therapeutic or mock vector at age 1 month (n = 10 per group) and WT mice (n = 5). In all PNS tissues evaluated, improvement of myelination in treated in contrast to mock-treated *Sh3tc2*$^{-/-}$ mice was observed but without reaching WT levels. In lumbar roots (Figures 4A–M), g-ratios of all myelinated fibers in the treated group were 0.72 ± 0.02 compared with 0.78 ± 0.01 in the mock-treated group and 0.64 ± 0.01 in WT mice, while in fibers >4 μm in diameter g-ratio reached 0.80 ± 0.01 in treated compared with 0.84 ± 0.01 in the mock group and 0.70 ± 0.004 in WT. Average myelin thickness in treated mice was 0.50 ± 0.03 μm, in the mock group 0.40 ± 0.02 μm, and in the WT 0.64 ± 0.01, while the subset of fibers >4 μm reached myelin thickness of 0.55 ± 0.04 μm in treated compared with 0.40 ± 0.03 μm in mock-treated mice and 0.70 ± 0.01 in WT mice. Furthermore, the percentage of demyelinated fibers was significantly reduced in treated mice to 0.02 ± 0.003 compared with 0.04 ± 0.004 in the mock group (0.0003 ± 0.0003 in the WT group).

In femoral motor nerves (Figures 4N–4Z), g-ratios reached 0.66 ± 0.02 in treated compared with 0.70 ± 0.02 in mock-treated mice (0.65 ± 0.01 in WT mice), while in fibers >4 μm in diameter the corresponding g-ratios were 0.77 ± 0.01 (treated), 0.81 ± 0.01 (mock), and 0.70 ± 0.01 (WT). Average myelin thickness was 0.57 ± 0.03 μm in the treated group, 0.42 ± 0.02 mm in the mock group (0.74 ± 0.02 in WT group) and, in fibers >4 μm, 0.62 ± 0.03 μm in the treated group compared with 0.49 ± 0.03 μm in the mock group (0.98 ± 0.03 in the WT mice). As in the lumbar roots, the ratio of demyelinated fibers decreased to 0.02 ± 0.002 in treated compared with 0.04 ± 0.01 in the mock group (0.00 ± 0.00 in WT).

Finally, morphological analysis of mid-sciatic nerves (Figure S2) confirmed improvement in g-ratios in treated mice (0.68 ± 0.01) compared with mock group (0.72 ± 0.01) (0.65 ± 0.01 in WT). In the fibers with diameter >4 μm, fully treated mice showed improved g-ratio of 0.78 ± 0.02 compared with 0.83 ± 0.01 in the mock group without reaching WT levels (0.67 ± 0.01). Average myelin thickness in treated mice was 0.44 ± 0.02 μm and in the mock group 0.40 ± 0.02 μm, both significantly lower than in WT mice (0.83 ± 0.13 μm), while fibers >4 μm in diameter showed increased myelin thickness of 0.51 ± 0.01 μm in treated compared with mock-treated animals (0.42 ± 0.01 μm) but did not reach WT thickness (1.2 ± 0.1 μm). As observed in other PNS tissues, complete demyelination was significantly decreased in the treatment group reaching a ratio of 0.01 ± 0.002, in contrast to 0.02 ± 0.01 in the mock-treated mice (0.005 ± 0.01 in WT). Axonal profiling analysis revealed a shift of axonal diameter distribution toward the population of smaller axons (<2 μm) in *Sh3tc2*$^{-/-}$ sciatic nerves compared with WT nerves, and this shift was significantly reduced in treated compared with mock-treated Sh3tc2$^{-/-}$ mice (Figure S2N). The observed profile changes, likely reflecting hypomyelination, did not lead to significant axonal loss in either treated or mock-treated animals compared with WT, as determined by similar total number of axons per nerve in all groups (Figure S2O).

Late treatment improves functional outcomes in older CMT4C mice

Following the completion of the early-treated trial in 1-month-old *Sh3tc2*$^{-/-}$ mice, and to confirm that therapeutic intervention at later stages of the neuropathy could also be beneficial in the CMT4C model, we also performed a randomized, mock-vector controlled treatment trial in 4-month-old *Sh3tc2*$^{-/-}$ mice. The level of phenotypic rescue in treated animals was compared with mock-treated littermates and age-matched WT mice by motor-behavioral, electrophysiological, and morphological studies 4 months after treatment in two groups (n = 20 per group) of *Sh3tc2*$^{-/-}$ mice and WT mice (n = 4–6 per group). Behavioral testing was carried out before treatment as well as at age 6 and 8 months (2 and 4 months after injection, respectively). At 8 months of age, mice were evaluated either by electrophysiological study or for quantitative morphometric analysis (n = 10 for each outcome measure per group and n = 4–6 WT mice)

Figure 3. Functional improvements after early treatment in *Sh3tc2*$^{-/-}$ mice

(A) Early treatment trial design and outcome measures used. (B) Vector genome copy numbers following intrathecal injection obtained from *Sh3tc2*$^{-/-}$ mice 2 months after injection (n = 7 per group) (R, lumbar roots; S, sciatic nerve). (C) Quantification of gene expression rates (% SH3TC2-expressing cells) in bilateral sciatic nerves and lumbar spinal roots of full vector injected mice (n = 4 mice). (D–I) Improved behavioral performance of *Sh3tc2*$^{-/-}$ mice treated at age 1 month with the full (SH3TC2) compared with the mock vector approaching WT levels, including time spent on rotarod at 20 (D–F) and 32 (G–I) rotations per minute (rpm), as well as hindlimb foot grip strength (J–L). (M and N) Electrophysiological analysis in 3-month-old *Sh3tc2*$^{-/-}$ mice injected at age 1 month shows improved sciatic nerve motor conduction velocities (MNCV) (M) and a trend for improved compound muscle action potentials (CMAP) (N) in treated compared with mock-treated mice (n = 10/group), although not reaching WT levels (n = 6). (O and P) Trend for improvement of hindlimb clasping phenotype of treated *Sh3tc2*$^{-/-}$ mice compared with mock-treated littermates and age-matched WT, as shown in representative images in (O) and by quantification of hindlimbs opening angle in (P). (Q) Improvement of nodal phenotype in treated *Sh3tc2*$^{-/-}$ mice. Immunostaining of sciatic nerve teased fibers from mock- or full vector-treated *Sh3tc2*$^{-/-}$ and WT *Sh3tc2*$^{+/+}$ mice, as indicated, shows the normal appearance of Nav1.6 (red, white arrows)-labeled node of Ranvier surrounded by Caspr immunoreactivity at paranodes (green, white open arrowheads) in the fibers from fully treated *Sh3tc2*$^{-/-}$ similar to WT mice, as opposed to the elongated nodal profile in fibers from mock-treated *Sh3tc2*$^{-/-}$. (R) Quantification of nodal length in groups of mice (>50 nodes counted per animal) confirms the correction of nodal pathology in treated *Sh3tc2*$^{-/-}$ mice. Values represent the mean ± SEM. *p < 0.05, **p < 0.01, ***p < 0.001 (unpaired, one-tailed Student's t test in B and C; all other comparisons one-way ANOVA with Tukey's multiple-comparison test). Scale bar, 10 μm.

Please cite this article in press as: Georgiou et al., AAV9-mediated *SH3TC2* gene replacement therapy targeted to Schwann cells for the treatment of CMT4C, Molecular Therapy (2023), https://doi.org/10.1016/j.ymthe.2023.08.020

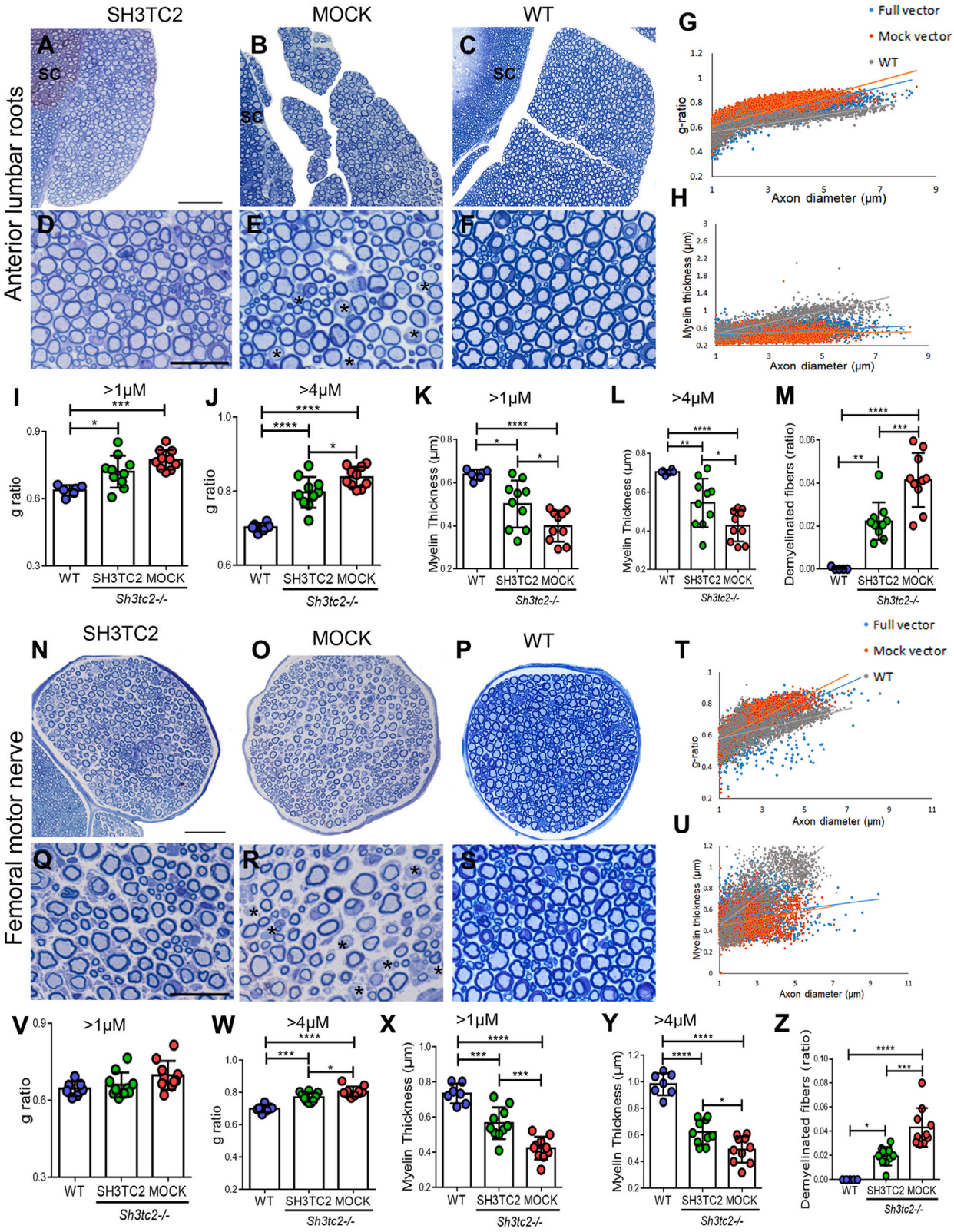

(legend on next page)

Please cite this article in press as: Georgiou et al., AAV9-mediated *SH3TC2* gene replacement therapy targeted to Schwann cells for the treatment of CMT4C, Molecular Therapy (2023), https://doi.org/10.1016/j.ymthe.2023.08.020

(Figure 5A). Examiners were blinded to the treatment status in all outcome measures.

To confirm vector biodistribution in older mice, VGCNs were determined 4 months post-injection in PNS tissues (n = 5 mice) and reached 0.92 ± 0.41 in anterior lumbar roots and 0.49 ± 0.25 in sciatic nerves (Figure 5B). The percentage of SH3TC2-expressing cells reached an average of 67.38% ± 3.4% in anterior lumbar roots and 67.04% ± 2.7% in sciatic nerves (n = 4 mice; Figure 5C). Comparison of rotarod test performance over time showed that AAV9-mini*Mpz.SH3TC2myc* treatment improved motor performance in *Sh3tc2*$^{-/-}$ mice compared with mock-treated littermates without reaching the level of WT mice. (Figures 5D–5K). Foot grip strength was also significantly increased 4 months post-injection in fully treated mice compared with the mock group approaching WT performance (Figures 5L–5O). Moreover, late treatment with AAV9-mini-*Mpz.SH3TC2myc* fully reversed the hindlimb clamping abnormality of *Sh3tc2*$^{-/-}$ mice (Figures 5P and 5Q).

Nerve conduction studies in the *Sh3tc2*$^{-/-}$group at the age of 8 months, 4 months after treatment (Figures 5R and 5S), revealed significantly increased sciatic MNCVs in AAV9-mini*Mpz.SH3TC2myc*-treated mice (32.34 ± 1.61 m/s) compared with the mock group (25.35 ± 1.35 m/s) but without reaching WT levels (39.59 ± 0.84 m/s). Moreover, the sciatic nerve CMAP amplitude was significantly higher in treated (4.75 ± 0.39 mV) compared with mock-treated *Sh3tc2*$^{-/-}$ mice (3.08 ± 0.30 mV) approaching WT values (5.23 ± 0.33 mV).

Nodal pathology in CMT4C mice improves also after late treatment

Given the functional improvements, we further examined whether the early-onset nodal pathology that is characteristic of CMT4C could also be improved following delayed gene replacement. Morphometric analysis of sciatic nerve teased fibers from 8-month-old *Sh3tc2*$^{-/-}$ mice (4 months after vector injection) which were double labeled for axonal nodal and paranodal markers Nav1.6 and Caspr, respectively. We observed that the typical nodal elongation found in nerve fibers from mock-treated *Sh3tc2*$^{-/-}$ mice was improved in treated littermates and did not differ from nodal morphology in WT nerves (Figure 5T). Quantification of nodal length of 50 nodes per mouse from n = 10 mock and n = 10 fully treated *Sh3tc2*$^{-/-}$ mice, as well as from n = 3 WT mice confirmed these observations (Figure 5U).

Late treatment improves myelination in the model of CMT4C

As in early-treatment groups, morphological examination in transverse semithin sections of anterior lumbar roots and femoral motor and mid-sciatic nerves from 8-month-old *Sh3tc2*$^{-/-}$ mice treated at age 4 months showed improved myelination in all PNS tissues of treated in contrast to mock-treated *Sh3tc2*$^{-/-}$ mice but without reaching WT levels. In anterior lumbar roots (Figures 6A–M) the g-ratio of myelinated fibers of >1 in diameter in fully treated mice was 0.73 ± 0.01 in comparison with 0.76 ± 0.01 in the mock group and 0.64 ± 0.01 in the WT group, while the subset of fibers >4 μm in diameter showed a g-ratio of 0.83 ± 0.01 in treated compared with 0.85 ± 0.01 in the mock-treated mice and 0.69 ± 0.02 in WT mice. Average myelin thickness in treated mice reached 0.45 ± 0.01 μm and in the mock group 0.39 ± 0.02 μm compared with 0.86 ± 0.06 in WT, while in fibers >4 μm myelin thickness improved to 0.46 ± 0.01 μm in treated mice compared with 0.40 ± 0.02 μm in the mock group but remained lower that in WT mice (1.08 ± 0.04). Furthermore, treated mice showed reduced ratios of demyelinated fibers reaching 0.05 ± 0.01 compared with 0.08 ± 0.01 in the mock group although remaining higher than in WT (0.02 ± 0.003).

Moreover, in femoral motor nerves of late-treated *Sh3tc2*$^{-/-}$ mice (Figures 6N–6Z) g-ratios reached 0.68 ± 0.01 compared with 0.72 ± 0.01 in the mock group and approached WT values (0.64 ± 0.01), while in fibers with diameter >4 μm g-ratio in treated mice was 0.78 ± 0.01 and in mock-treated mice 0.81 ± 0.01 compared with 0.7 ± 0.01 in WT. Average myelin thickness improved in the treated group (0.56 ± 0.02 μm) compared with the mock group (0.47 ± 0.02 μm) but did not reach WT thickness (0.8 ± 0.04), while in the subset of fibers >4 μm the myelin thickness increased to 0.63 ± 0.02 μm in treated compared with 0.52 ± 0.03 μm in mock-treated mice again without reaching WT levels (1.04 ± 0.06). The demyelinated fiber ratio decreased to 0.02 ± 0.002 as opposed to 0.04 ± 0.004 in mock-treated animals (0.00 ± 0.00 in the WT group).

Finally, morphological analysis of mid-sciatic nerves (Figure S3) confirmed significant improvement in late-treated mice reaching

Figure 4. Improved PNS myelination in early-treated CMT4C mice

Toluidine blue-stained semithin sections of anterior lumbar spinal roots attached to the spinal cord (A–F) and femoral motor nerves (N–S) at low (upper panels) and higher (lower panels) magnification from 3-month-old *Sh3tc2*$^{-/-}$ mice injected at age 1 month with AAV9-mini*Mpz.SH3TC2myc* or with AAV9-mini*Mpz.EGFP* (mock) vector and WT mice as indicated. (G–M) Morphometric analysis of anterior lumbar roots (n = 10 mice per treatment group and n = 6 mice for WT group) including scatterplots displaying as indicated g-ratios (G) and myelin thickness (H) of individual axons versus axonal diameter (red points, mock-treatment group; blue points, full-treated group; gray points, WT group; each point corresponds to one fiber). Comparison of g-ratios from all fibers >1 μm in diameter (I), as well as from the subset of fibers >4 μm diameter (J), shows a trend for reduction in >1 μm and significant reduction in >4-μm fibers from treated compared with mock-treated mice, while the corresponding myelin thickness is increased (K and L), without complete correction to WT levels. The ratio of completely demyelinated fibers (M) is also reduced in treated compared with mock-treated *Sh3tc2*$^{-/-}$ mice. (N–Z) Morphometric analysis of femoral motor nerves (n = 10 per treatment group and n = 7 for WT) including scatterplots of g-ratios (T) and myelin thickness (U) of individual axons versus axonal diameter and comparison of g-ratios from all fibers >1 μm in diameter, as well as from the subset of fibers >4 μm, shows a trend for g-ratio reduction in fibers >1 μm (V) and significant reduction in >4-μm fibers (W) in fully treated compared with mock-treated mice, while the corresponding myelin thickness is increased (X and Y). The ratio of completely demyelinated femoral fibers (Z) is also reduced in treated compared with mock-treated *Sh3tc2*$^{-/-}$ mice. None of the myelination improvements reaches the level of WT tissues. Values represent mean ± SEM; one-way ANOVA with Tukey's multiple-comparison test. Scale bars, 50 μm in (A–C and N–P) and 25 μm in (D–F and Q–S).

Please cite this article in press as: Georgiou et al., AAV9-mediated *SH3TC2* gene replacement therapy targeted to Schwann cells for the treatment of CMT4C, Molecular Therapy (2023), https://doi.org/10.1016/j.ymthe.2023.08.020

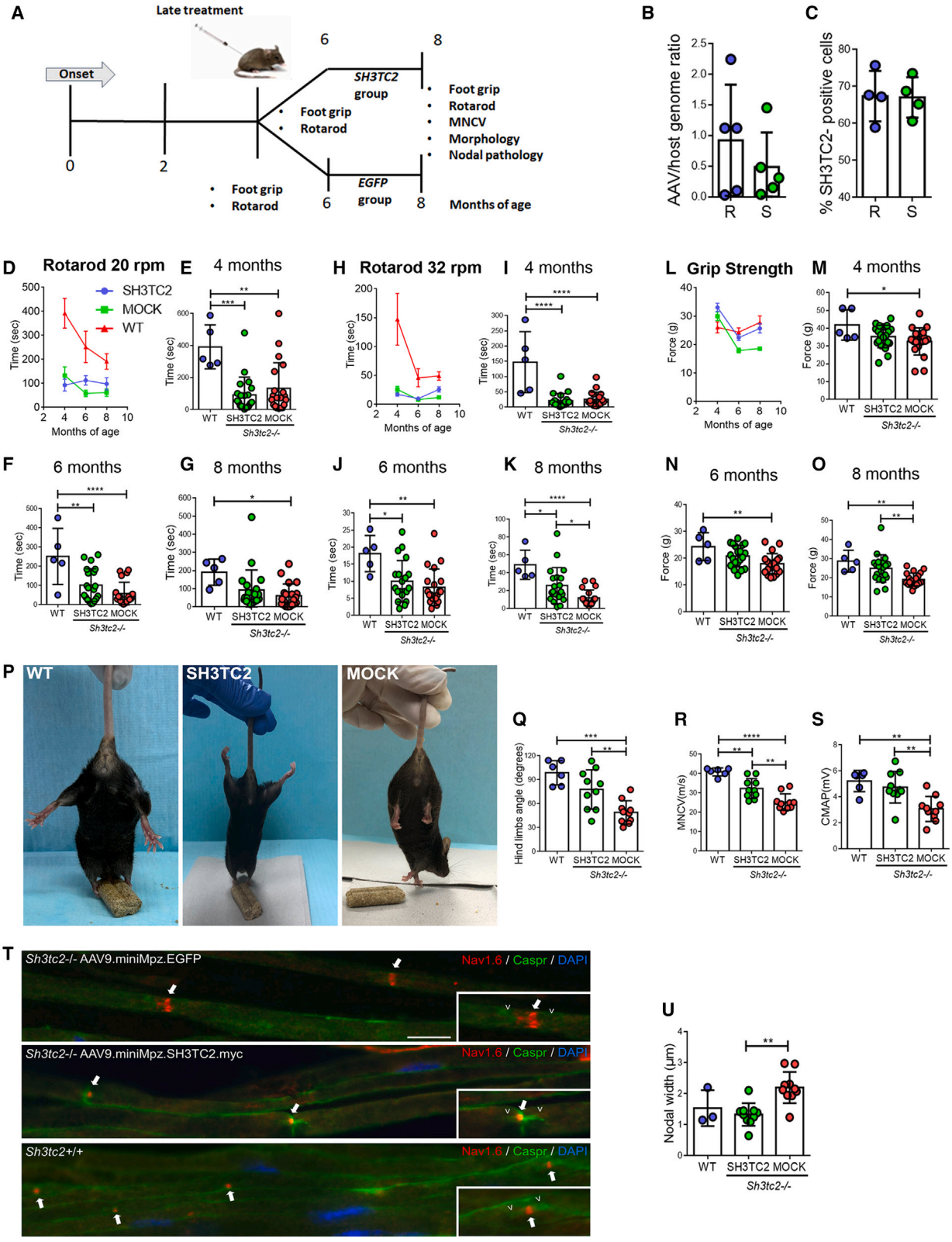

(legend on next page)

Please cite this article in press as: Georgiou et al., AAV9-mediated *SH3TC2* gene replacement therapy targeted to Schwann cells for the treatment of CMT4C, Molecular Therapy (2023), https://doi.org/10.1016/j.ymthe.2023.08.020

g-ratios of 0.69 ± 0.01 compared with 0.72 ± 0.06 in mock-treated littermates remaining above WT values of 0.64 ± 0.02, while in the fibers with diameter >4 μm, fully treated mice showed a g-ratio of 0.8 ± 0.0042 compared with 0.83 ± 0.004 in the mock group, whereas WT showed values of 0.68 ± 0.01. Average myelin thickness reached 0.46 ± 0.01 μm in treated and 0.40 ± 0.01 μm in mock-treated *Sh3tc2*$^{-/-}$ mice without reaching WT levels (0.68 ± 0.03), while in the subset of fibers >4 μm in diameter myelin thickness reached 0.51 ± 0.02 μm in the treatment group in comparison with 0.42 ± 0.01 μm in the mock-treated mice but did reach WT levels (1.02 ± 0.04). Moreover, a significant reduction in the ratios of completely demyelinated fibers was found in the sciatic nerves of the treated group (0.01 ± 0.002) in comparison with the mock group (0.02 ± 0.005) approaching the WT (0.008 ± 0.001). As in early-treated groups, sciatic nerve axonal profiling revealed a shift toward smaller axons (<2 μm) in *Sh3tc2*$^{-/-}$ sciatic nerves compared with WT nerves, with a trend for improvement in the treated mice while the total number of axons per nerve was similar in all groups (Figures S3N–S3O).

Plasma NF-L levels in CMT4C mice over time and after treatment

Blood samples were obtained from 3- and 8-month-old untreated *Sh3tc2*$^{-/-}$ and age-matched WT mice (n = 5 per genotype), as well as from fully treated and mock-treated mice in both early- and late-treatment trials (n = 4 per time point and treatment condition) and from age-matched WT (n = 4), prior to sacrificing using standard methods. Baseline assessment in untreated *Sh3tc2*$^{-/-}$ mice showed significant NF-L elevation compared with WT mice at age 3 months. Interestingly, although this NF-L elevation in *Sh3tc2*$^{-/-}$ mice persisted at age 8 months, it showed no progression, but instead a significant drop compared with the 3-month-old group (Figure S4A). Comparison of NF-L levels in early-treated mice (n = 4 per group) showed a trend for improvement in treated compared with mock-treated 3-month-old *Sh3tc2*$^{-/-}$ mice but did not reach WT levels (Figure S4B), and a similar trend for NF-L reduction in late-treated 8-month-old animals compared with the corresponding mock group approaching WT levels (Figure S4C).

DISCUSSION

CMT4C is the most prevalent recessively inherited demyelinating neuropathy and arises from loss-of-function mutations in the *SH3TC2* gene. In this study, we have developed a gene therapy approach to treat CMT4C by using a minimal version of the myelin-specific rat *Mpz* promoter (mini*Mpz*) to drive human *SH3TC2* gene expression restricted to Schwann cells. In previous work, we developed a lentiviral vector system to express the *SH3TC2* coding sequence under the control of the full-length Mpz promoter. LV-*Mpz.SH3TC2myc* was delivered only at early stages of the neuropathy into 3-week-old *Sh3tc2*$^{-/-}$ mice by lumbar intrathecal injection leading to adequate Schwann cell-specific gene expression and therapeutic benefit.[18] However, the limitations of *in vivo* lentiviral vector delivery[25] motivated us to explore as a clinically more translatable approach the possibility of delivering the therapeutic *SH3TC2* gene using the AAV9 vector that has shown better biodistribution, improved safety profile, and higher expression levels in the PNS.[22,32] Here, the AAV9-mediated approach resulted in widespread Schwann cell targeting throughout the PNS leading to significant functional and morphological improvements in the *Sh3tc2*$^{-/-}$ mouse model of CMT4C, not only with early treatment at age 1 month, but also when delivered at much later stages of the neuropathy at the age of 4 months. The efficacy of this gene therapy approach was demonstrated using multiple functional and pathological outcome measures that are relevant not only for the phenotype of this model[13] but also for the human disease CMT4C.[5,6,12]

Our results confirm that a minimal version of the rat *Mpz* promoter can provide strong gene expression specifically in myelinating Schwann cells. Minimal promoters are short sequences that retain transcriptional control elements allowing for the formation of the initiation complex, and can maximize the transgene capacity of recombinant AAV vector genomes (vgs).[33–35] Previous work has indicated that most of the functional regulatory elements and crucial transcription factor binding sites, including that of SOX10 and EGR2, are located within this distal promoter fragment downstream of the AvrII site.[31] Thus, we PCR amplified this 412-bp-long sequence and validated its efficacy and fidelity initially through evaluation of the reporter gene expression. Similar to the full-length *Mpz* promoter tested previously,[18,22,32,36] we showed that a high percentage of myelinating Schwann cells was expressing EGFP in the PNS. At the same time, in the CNS, less than 2% of neurons in the lumbar spinal cord and a very low percentage of oligodendrocytes were EGFP positive, confirming

Figure 5. Functional improvements after late treatment in *Sh3tc2*$^{-/-}$ mice

(A) Delayed treatment trial design and outcome measures used. (B) Vector genome copy numbers obtained from *Sh3tc2*$^{-/-}$ mice 4 months following intrathecal injection (n = 5 per group) (R, lumbar roots; S, sciatic nerve). (C) Quantification of SH3TC2 expression rates in bilateral sciatic nerves and lumbar spinal roots from n = 4 mice injected with the full vector. (D–O) Improved behavioral performance of *Sh3tc2*$^{-/-}$ mice treated with the full (SH3TC2) compared with the mock vector, including time spent on rotarod at 20 (D–G) and 32 (H–K) rpm, and hindlimb foot grip strength (L–O), although not reaching the level of WT mice performance in most tests. (P–Q) Improvement of hindlimb clasping phenotype of late-treated compared with mock-treated *Sh3tc2*$^{-/-}$ and WT mice, examined at age 8 months, as shown in representative images in (P) and by quantification of hindlimbs opening angle in (Q). (R and S) Electrophysiological analysis in 8-month-old *Sh3tc2*$^{-/-}$ mice injected at age 4 months shows improved sciatic MNCV (R) as well as CMAPs (S) in treated compared with mock-treated mice, although velocities remain lower than in WT controls (n = 10/treatment group and n = 6 for WT). (T) Improvement of nodal phenotype in late-treated *Sh3tc2*$^{-/-}$ mice. Immunostaining of sciatic nerve teased fibers from mock- or full vector-treated *Sh3tc2*$^{-/-}$ and WT mice, as indicated, shows the normal appearance of Nav1.6 (red, white arrowheads)-labeled node of Ranvier surrounded by Caspr immunoreactivity at paranodes (green, white open arrowheads) in the fibers from fully treated *Sh3tc2*$^{-/-}$ similar to WT mice, as opposed to the elongated nodal profile in fibers from mock-treated *Sh3tc2*$^{-/-}$ animals. (U) Quantification of nodal length in groups of mice (>50 nodes counted per animal) confirms the correction of nodal pathology in late-treated animals. Values represent the mean ± SEM. *p < 0.05, **p < 0.01, ***p < 0.001 (unpaired, one-tailed Student's t test in B and C; for all other comparisons one-way ANOVA with Tukey's multiple-comparison test). Scale bar, 10 μm.

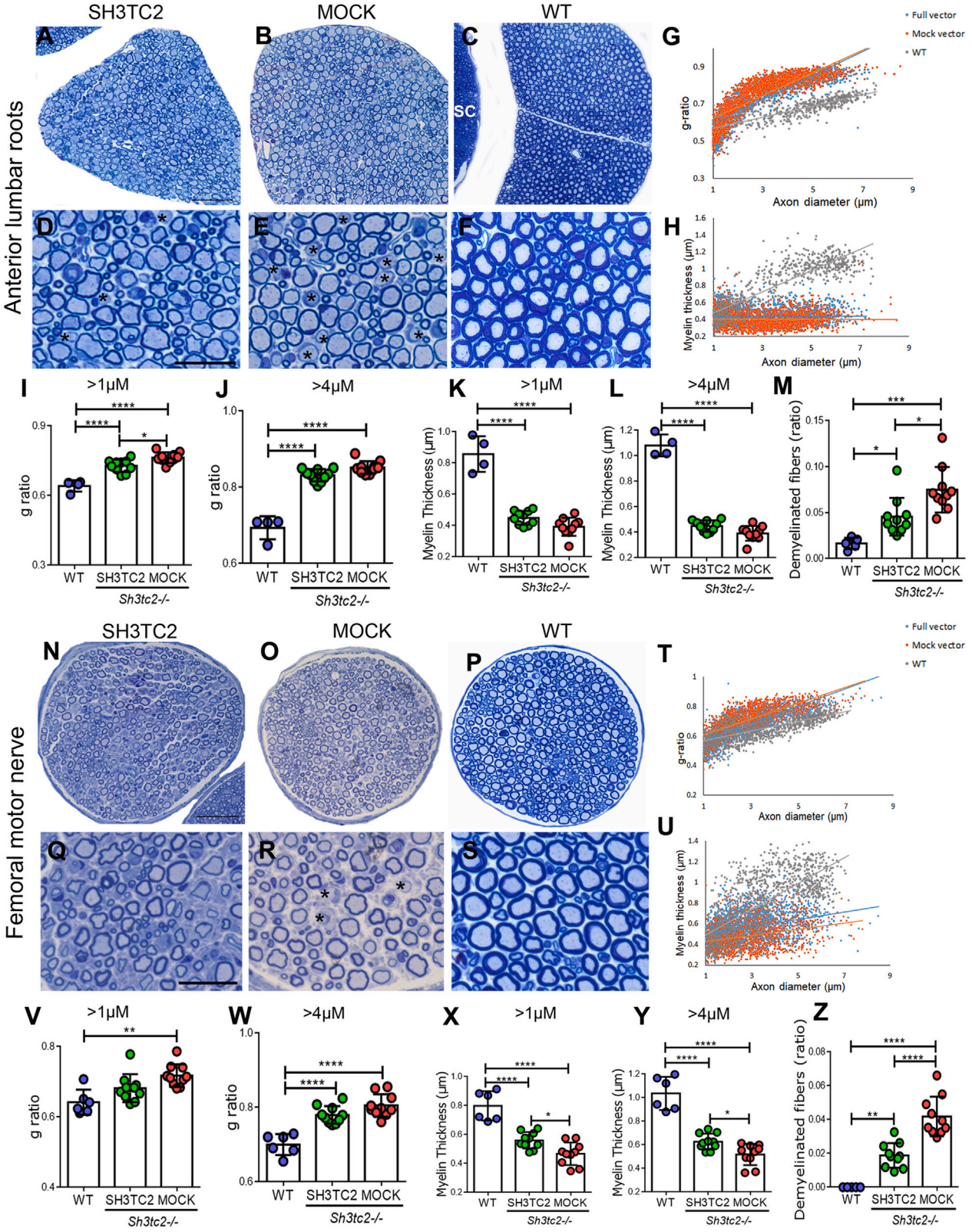

(legend on next page)

Please cite this article in press as: Georgiou et al., AAV9-mediated *SH3TC2* gene replacement therapy targeted to Schwann cells for the treatment of CMT4C, Molecular Therapy (2023), https://doi.org/10.1016/j.ymthe.2023.08.020

the largely preserved specificity of this reduced promoter version to restrict expression in Schwann cells. Thus, we provide strong evidence for the usefulness of this minimal PNS myelin-specific promoter to facilitate packaging of larger coding sequences into the AAV expression cassette that can be utilized not only for CMT4C treatment, but also for various gene therapy approaches to treat other demyelinating CMT neuropathies.

AAV vectors have emerged as leading tools for delivering *in vivo* gene therapies to treat a variety of diseases[19,22,23,37–39] due to their efficient biodistribution and proven safety profile.[40] Many AAV-based gene therapy clinical trials are underway or have been completed with more than 3,000 patients treated in the past 20 years, providing accumulating clinical experience in AAV gene therapy.[41] Among AAV serotypes, AAV9 is one of the most frequently used serotypes in gene therapy programs for neurological disorders, due to its ability to cross the blood-brain barrier (BBB) and to diffuse within the brain parenchyma, leading to efficient transduction of neural cells.[39] This vector has been used to accomplish extensive and long-lasting expression of therapeutic transgenes through intra-CSF delivery in various models including those of SMA and Krabbe's disease.[42,43] Furthermore, it efficiently crosses the BBB when administered intravenously, at least in infants, and has been applied in preclinical and clinical treatments for SMA[26,44–46] and Canavan disease.[47] Efficient CNS targeting has also been demonstrated in large animals at different ages.[48] Importantly, AAV9 has been shown to target efficiently the PNS via intrathecal,[22,28,32] intravenous,[32] or intraneural administration,[49] with high degree of tropism for myelinating Schwann cells leading to therapeutic *GJB1* gene expression controlled by the Schwann cell-specific Mpz promoter to treat CMT1X neuropathy,[22,32] or to *PMP22* gene silencing by shRNA[49] or microRNA[28] under ubiquitous promoters.

In this study, we achieved widespread expression of EGFP or SH3TC2 in Schwann cells in various PNS tissues following lumbar intrathecal injection of AAV9 vector. Both the analysis of VGCNs biodistributed to the PNS tissues, as well as the percentage of transduced Schwann cells expressing the reporter or the therapeutic gene in lumbar roots and in sciatic nerves indicates a gradient of biodistribution from the site of injection, as in our previous studies.[22,32] Nevertheless, the lumbar intrathecal delivery provides important advantages for clinical translation of PNS treatments, due to the five times lower amount of vector needed compared with intravenous delivery,[32] and minimal invasiveness with more widespread expression compared with the direct intraneural injection.[30,49] In addition, we demonstrate that AAV9-delivered SH3TC2 localizes correctly to the perinuclear cytoplasm of myelinating Schwann cells of the PNS as shown before with lentiviral delivery.[18] Although the overall VGCNs and SH3TC2 expression rates were not very high in the sciatic nerves, they were still sufficient to produce significant therapeutic effects in the CMT4C model. However, we acknowledge that phenotype rescue was not complete, similar to the results obtained previously in the CMT4C, CMT1X, and CMT1A models.[18,22,28,36,50] In fact, both in the functional and electrophysiological outcome measures, as well as in the morphological analysis of myelination, treated *Sh3tc2*$^{-/-}$ mice mostly failed to reach the levels of age-matched WT control mice. This may reflect the severity and early onset of the pathology in this model, as well as the partial Schwann cell correction by gene delivery.

The *Sh3tc2*$^{-/-}$ mice develop a gradually worsening peripheral neuropathy characterized by hypomyelination and slowing of motor and sensory nerve conduction velocities.[13] This mouse model reproduces the major phenotypic features of the human disease, while retaining fertility and normal lifespan. To evaluate functional improvement after treatment, we applied both rotarod and foot grip strength analysis, which were shown to be treatment responsive in our previous experiments using this mouse model[18] and in other models of peripheral neuropathy.[22,28,36,50] Both of these tests confirmed significant improvement in the motor performance of treated compared with mock-treated *Sh3tc2*$^{-/-}$ mice both at the early as well as at the late treatment time points. Consistent with these behavioral improvements, sciatic MNCV was also increased in treated *Sh3tc2*$^{-/-}$ mice. Although early- and late-treatment groups were not examined in parallel, thus precluding a direct comparison, their functional improvements were of similar magnitude, albeit not reaching WT levels, suggesting that even with delayed treatment some of the pathological changes already established in aged animals can be at least partially reversed. Interestingly, the CMAP improvement was only significant in the late-treatment groups, likely because at this age secondary axonal pathology and muscle denervation is more pronounced than in 3-month-old CMT4C mice, allowing for a clearer treatment effect to be obtained. In addition, late-treated mice were evaluated 4 months

Figure 6. Improved PNS myelination in late-treated CMT4C mice

Toluidine blue-stained semithin sections of anterior lumbar spinal roots attached to the spinal cord (A–F) and femoral motor nerves (N–S) at low (upper panels) and higher (lower panels) magnification from 8-month-old *Sh3tc2*$^{-/-}$ mice injected at age 4 months with AAV9-mini*Mpz*.*SH3TC2myc* or with AAV9-*miniMpz*.*EGFP* (mock) vector as indicated as well as age-matched WT mice as controls. (G–M) Morphometric analysis of anterior lumbar roots (n = 10 mice per group and n = 4 for WT group) including scatterplots displaying as indicated g-ratios (G) and myelin thickness (H) of individual axons versus axonal diameter (red points, mock-treatment group; blue points, full-treated group; gray points, WT group; each point corresponds to one fiber). Comparison of g-ratios from all fibers >1 μm in diameter (I), as well as from the subset of fibers >4 μm (J) shows reduction in treated compared with mock-treated mice, while the corresponding myelin thickness tends to increase (K and L), although all parameters remain below WT levels. The ratio of completely demyelinated fibers (M) is also reduced in treated compared with mock-treated *Sh3tc2*$^{-/-}$ mice but still higher than in WT animals. (N–S) Morphometric analysis of femoral motor nerves (n = 10 per treatment group and n = 6 for WT) including scatterplots of g-ratios (T) and myelin thickness (U) of individual axons versus axonal diameter and comparison of g-ratios shows reduction of g-ratios in both >1-μm (V) and in >4-μm fibers (W) in treated compared with mock-treated mice, while the corresponding myelin thickness is increased (X and Y). The ratio of completely demyelinated fibers (Z) is also reduced in late-treated compared with mock-treated *Sh3tc2*$^{-/-}$ mice. None of myelination parameters reaches WT levels. Values represent mean ± SEM (one-way ANOVA with Tukey's multiple-comparison test). Scale bars, 50 μm in (A–C and N–P) and 25 μm in (D–F and Q–S).

after treatment, as opposed to 2 months in early groups, which may account for clearer CMAP response.

Functional improvements in treated CMT4C mice were reflected in the improvement of key morphological abnormalities, including the nodal pathology. Elongation of the nodes of Ranvier in peripheral myelinated fibers is a characteristic pathological feature of CMT4C neuropathy revealed by patient nerve biopsies, and has also been observed in as early as postnatal day 8 in *Sh3tc2*$^{-/-}$ mice, along with disrupted axon-glial junctions.[13,18] The observed elongation of the nodes is predicted to contribute to the reduction of conduction velocity in myelinated axons in CMT4C patients and in this model,[51] while reversal of this abnormality likely accounts in part for the improved sciatic nerve conduction velocities. The organization of the nodal region during which sodium channel clustering is the main objective, relies on a dual cellular mechanism. First, the interaction of adhesion molecules neurofascin186, NrCAM, and gliomedin at the node, and, second, the formation of paranodal axon-glial junctions by Caspr, contactin, and NF155 preventing the lateral movement of sodium channels away from the node.[52,53] In CMT4C-associated nodal pathology, Nav1.6 channels remain clustered within the elongated nodes, indicating that the above mechanisms are not disrupted, but rather a defect in the lateral growth of Schwann cells is likely to cause the observed nodal widening during myelination.[13] SH3TC3 has been shown to interact with Rab11 and to play a crucial role in the endocytic recycling system.[54,55] During myelination, specialized microtubule networks are observed in Schwann cells, suggesting increased rates of vesicle transport.[56,57] For myelin membrane formation, various proteins have to be sorted and guided to distinct plasma membrane domains using endosomal pathways.[58] Thus, disruption of the endocytic recycling system in CMT4C may lead to impaired Schwann cell elongation and wider nodal gap, while myelin growth and thickness is also defective. Interestingly, in this study we observed that this early nodal phenotype improves not only in *Sh3tc2*$^{-/-}$ mice treated early in the disease course, but also after late treatment, confirming that developmental Schwann cell defects can be reversible. Thus, re-establishing SH3TC2 expression led to a considerable remodeling of the nodal architecture reaching that of WT nerves. This may in fact be a more responsive therapeutic outcome and could account in part for the functional improvements such as increased nerve conduction velocities observed in our study. In contrast, myelin thickness remained well below WT levels, likely accounting for the lack of full MNCV correction.

The morphometric evaluation of lumbar motor roots and femoral and mid-sciatic nerves focused on assessment of the hypomyelination phenotype of *Sh3tc2*$^{-/-}$ mice and revealed improvement in g-ratios as well as in the average myelin thickness, in addition to reduced ratios of completely demyelinated fibers. *Sh3tc2*$^{-/-}$ mice present with hypomyelination as early as 1 month of age, with slowly progressive demyelination ensuing overtime,[13] indicating that a combination of developmental and progressive abnormalities in myelination create the neuropathy in this model. Here we demonstrate significant but only partial improvement compared with WT in most myelination parameters both in early- as well as in late-treatment groups. As in our previous work,[18] these improvements were more significant in the subset of myelinated fibers >4 μm in diameter, which are known to be more affected in this CMT4C model.[13] As with the nodal pathology, improvement in these early developmental myelin defects following the replacement of SH3TC2 function in Schwann cells confirms the potential for reversing myelin pathological abnormalities in CMT4C. However, it should be noted that axonal pathology is generally mild in this model,[13,59] in contrast to CMT4C patients who are likely to have accumulated axonal loss by early adulthood. Thus, in contrast to myelin pathology, reversal of axonal degeneration may be much more difficult to achieve in the clinical application.

Plasma NF-L levels are elevated in patients with several types of CMT neuropathies with notable exception of CMT2E.[60] Elevated NF-L levels were also found in CMT mouse models, and showed responsiveness to at least early treatment,[22,28] suggesting that this may be a valuable biomarker for CMT neuropathies. In our previous study, we demonstrated that plasma NF-L was increased in *Sh3tc2*$^{-/-}$ mice with increasing age from 6 to 25 weeks.[18] This study essentially replicates those findings in older age groups at 12 and 32 weeks. However, we also observed here a significant drop in NF-L levels in older mice not previously appreciated, indicating that NF-L levels do not necessarily continue to increase with age in a predictable manner but may rather reflect the degree of active axonal pathology at any given age. A similar observation was made in the CMT1X model with peak NF-L levels at age 6 months and a decrease up to the age of 10 months (our unpublished observations), as well as in patients with various types of CMT neuropathies who showed a plateau or even reduction of initially elevated plasma NF-L levels over the years.[60] In this study, both the early as well as the late treatment groups showed a trend for reduction in NF-L levels compared with the mock groups, but without reaching statistical significance likely due to variations in and small numbers of animals examined. Nevertheless, our study further supports the use of plasma NF-L as a biomarker in CMT subtypes including CMT4C disease, which, depending on the stage of the neuropathy, may show an early response to treatment, if not a stable amelioration in the long term.

In conclusion, we demonstrate that lumbar intrathecal injection, a clinically translatable route of administration, of a novel AAV9-mini*Mpz.SH3TC2myc* vector, provides a significant albeit partial therapeutic benefit in the CMT4C model. The AAV9 vector achieves a better biodistribution to the PNS and higher expression rates in Schwann cells compared with the previously used lentiviral vector, while offering an established safety profile of clinical applicability. Moreover, we show that the minimal version of the Mpz promoter largely retains efficacy while preserving cell specificity, providing a useful tool to design treatments for other demyelinating neuropathies as well. Improved functional and morphological outcomes were achieved both with early as well as with late treatment in the CMT4C model, confirming that myelination defects can be partially reversible even at advanced stages of the neuropathy. While this research provides encouraging data for a potential gene

Please cite this article in press as: Georgiou et al., AAV9-mediated *SH3TC2* gene replacement therapy targeted to Schwann cells for the treatment of CMT4C, Molecular Therapy (2023), https://doi.org/10.1016/j.ymthe.2023.08.020

replacement approach to treat CMT4C, further studies are needed to evaluate the optimal vector dose as well as to demonstrate the scale-up potential in larger animals.

MATERIAL AND METHODS

Cloning of the AAV9-mini*Mpz.EGFP* and AAV9-mini*Mpz.SH3TC2myc* vectors

For the cloning of the AAV9-mini*Mpz.EGFP* (mock) vector the expression plasmid pAAV-*Mpz.EGFP* described previously[22] was modified for the current research. A shorter version of myelin-specific promoter had to be generated because the *SH3TC2* coding sequence together with the full-length Mpz promoter would exceed the capacity of the AAV vectors (4.7 kb ITR to ITR). At first, we PCR amplified from the full rat Mpz promoter sequence the fragment that includes the distal 412-bp downstream of the AvrII site. This is the area where most of the functional regulatory elements of the promoter are located.[31] The fragment was ligated to the pAAV-*Mpz.EGFP* vector after excision of the full-length Mpz promoter using the KpnI and AgeI restriction sites (Figure 1A).

For the cloning of the therapeutic (full) vector AAV9-mini-*Mpz.SH3TC2myc*, the *SH3TC2myc* sequence[18] was ligated downstream of the mini*Mpz* promoter after excision of the reporter EGFP sequence. To optimize the expression cassette size for more efficient AAV packaging capacity, we performed further cloning to reduce the size of the construct. The ~3.9-kb cDNA of the human *SH3TC2/KIAA1985* coding sequence along with a C terminus myc-tag was inserted downstream of the mini*Mpz* promoter. The WPRE and the bGHpA elements were excised and replaced by a small synthetic poly(A) (72 bp), which was ligated using the NotI/HindIII sites: GGAGCTCTCGAGAGGCCTAATAAAGAGCTCAGATGCATCG ATCAGAGTGTGTTGGTTTTTTGTGTGAGATCT (Figure 2A). Correct assembly of the expression cassettes was confirmed by restriction digest mapping and by sequencing.

Vector productions

The pAAV-mini*Mpz.EGFP* and pAAV-mini*Mpz.SH3TC2myc* plasmids were cross-packaged into the AAV9 capsid as described previously.[22] In brief, HEK293T cells were transfected using the co-precipitation method with the adenovirus-helper plasmid, the transfer plasmid, and rep2 and cap9 plasmids. Forty-eight hours later the cells were pelleted by centrifugation and re-dissolved in lysis buffer and incubated at 37°C for 1 h. The lysate was filtered with the supernatant through 0.45-μm Millipore filters. RNAse A and a protease inhibitor cocktail were added to both the lysate and the supernatant and incubated for 2 h at 37°C. The virus-containing aqueous layer was transferred to a Beckmann UltraClear SW41 tube and centrifuged at 149,000 × *g* for 3 h. The aqueous layer was discarded and the viral pellet re-suspended in 200 μL pellet suspension buffer. Vector titers in vg/mL were determined by qPCR targeting either the WPRE sequence[61] in the mock vector reaching 1.5×10^{12} vg/mL, or the human *SH3TC2* coding sequence (Hs00226194_m1, Applied Biosystems) in the full vector reaching 8×10^{12} to 1.02×10^{13} vg/mL.

Experimental mice

The intrathecal gene delivery experiments were conducted using WT C57BL/6 or *Sh3tc2*$^{-/-}$ mice. The generation and characterization of the *Sh3tc2*$^{-/-}$ mouse model has been described previously.[13,18] All animals were kept under specific pathogen free, standard controlled conditions of temperature (21°C–23°C), humidity, air exchange and light cycle (12/12 h light/dark) and provided with standardized mouse diet and drinking water *ad libitum*. All experimental procedures were conducted in accordance with animal care protocols approved by the Cyprus Government's Chief Veterinary Officer (project license CY/EXP/PR.L3/2017) according to national law and European guidelines (EC Directive 86/609/EEC).

Lumbar intrathecal injections

Vector delivery was performed under anesthesia by slow intrathecal injection into the L5-L6 intervertebral space of 1-, 2-, or 4-month-old mice as described previously.[32,36,50,62] In brief, following a small skin incision along the lower lumbar spine level to visualize the spine, the AAV9 vector was injected into the L5-L6 intervertebral space. A 50-μL Hamilton syringe connected to a 26-gauge needle was used to inject 20 μL of the vector stock containing an estimated total amount of 2×10^{11} vg. A flick of the tail was considered indicative of successful intrathecal administration.

Tissue processing and expression analysis

For immunofluorescence staining, mice were anesthetized with avertin according to institutionally approved protocols, and then transcardially perfused with phosphate-buffered saline (PBS) followed by fresh 4% paraformaldehyde (Merck, NJ) in 0.1 M PB buffer. The lumbar spinal cord with all roots attached as well as sciatic nerves were dissected and frozen for cryosections. Sciatic nerves were also teased into fibers under a stereoscope. Teased fibers or sections were permeabilized in cold acetone and incubated at room temperature with a blocking solution of 5% bovine serum albumin (Sigma-Aldrich, MO) containing 0.5% Triton X (Sigma-Aldrich) for 1 h. Mouse monoclonal primary antibodies used were: NeuN (1:400; Millipore, MA), CC1 (1:50; Millipore), GFAP (1:400; Abcam, Cambridge, UK), Caspr (1:100; Millipore). Rabbit polyclonal antibodies were used against SH3TC2 (1:50; Abcam), EGFP (1:1,000; Invitrogen, MA), Nav1.6 (1:100; Alomone, Jerusalem, Israel). Primary antibodies were incubated at 4°C overnight followed by appropriate secondary antibodies at room temperature. Slides were then washed in PBS and incubated with mouse cross-affinity fluorescein-conjugated (1:3,000; Invitrogen, A21202), rabbit fluorescein-conjugated (1:1,000; Jackson ImmunoResearch, 111-486-003), rabbit cross-affinity purified rhodamine-conjugated (1:3,000; Jackson ImmunoResearch, 111-026-003), and mouse cross-affinity purified rhodamine-conjugated (1:1,000; Jackson ImmunoResearch, 115-026-068) Slides were mounted with fluorescent mounting medium (DAKO) and images photographed under a fluorescence microscope (Nikon Eclipse Ni) with a digital camera (DS-Qi2) using NIS-Elements software.

Quantification of reporter gene EGFP (mock vector) or SH3TC2 (full vector) expression was performed at 5 weeks post-injection in ventral

lumbar spinal root sections and in sciatic nerve teased fibers (n = 5 mice) in images taken from five different areas in each slide. The number of EGFP- or SH3TC2-positive Schwann cells as well as the total number of cells in each picture was counted to determine the average expression ratio.

Determination of VGCNs

To assess vector biodistribution, genomic DNA was extracted from different PNS tissues (i.e., lumbar roots, proximal and distal sciatic nerves, and femoral motor nerves) of mice 8 or 16 weeks after intrathecal vector delivery using the MagPurix Tissue DNA Extraction Kit (Zinexts Life Science). The extracted DNA was analyzed for yield and purity using a NanoDrop 1000 spectrophotometer. DNA (5 μL) was used as a template for a duplex digital droplet PCR assay targeting either the EGFP or SH3TC2 gene of the transgene cassette and in parallel TFRC as a reference gene. Following droplet generation on a Bio-Rad QX200 AutoDG ddPCR system (Bio-Rad, France), the emulsion was transferred to a PCR plate and cycled using the following thermal cycler conditions: predenaturation at 95°C for 5 min, 40 cycles at 95°C for 30 s, 60°C for 1 min, and 4°C for 5 min, and a final step at 60°C for 10 min. Data acquisition and analysis were performed on a QX200 Droplet Reader and QuantaSoft Software (Bio-Rad). The VGCN was calculated from absolute ddPCR quantification as a ratio of the number of target copies to half the number of reference gene copies.

Treatment trial design at early and late time points

The aim of this study was to examine whether a gene addition therapy can improve the manifestations of peripheral neuropathy in the mouse model of CMT4C both at early as well as at late stages of the disease. *Sh3tc2*$^{-/-}$ mice were treated at the age of 1 month for the early treatment or at age 4 months for the late treatment. Littermate mice were randomized to either receiving the full vector AAV9-mini*Mpz.SH3TC2myc* treatment (treatment group, n = 20 per time point) or mock-vector AAV9-mini*Mpz.EGFP* (lacking the *SH3TC2* gene; serving as control group, n = 20 per time point) and were assigned a coding number for further identification. Randomization was based on animal numbering after tailing (mice with odd numbers randomized to full and mice with even numbers to mock treatment). To assess the level of correction, groups of age-matched WT mice were similarly evaluated as controls in all outcome measures.

In the early-treatment trial, 1-month-old mice were evaluated by behavioral testing by an examiner blinded to the treatment condition before treatment, and again at the age of 3 months, 2 months after treatment. In the late treatment trial 4-month-old mice were evaluated before treatment, and at the age of 6 and 8 months, 2 and 4 months after treatment, respectively. At the end of each trial mice were either evaluated by electrophysiology (n = 10 per treatment condition) or for quantitative morphometric analysis of semi-thin sections (n = 10 per treatment condition). Animals subjected to evaluation of nodal pathology were not used for morphological analysis. Analysis of physiological and morphological results was also performed blinded to the treatment condition.

Primary endpoint was considered the rescue of pathological changes in lumbar roots and peripheral nerves. Secondary endpoints were considered improvements in MNCVs and in motor test performance. Sample size estimation (individual animals) was based on minimum number that would enable robust non-parametric statistical analysis based on our previous studies using similar models.[18,30,32,36]

Motor behavioral analysis

Rotarod analysis

Each animal was placed daily for 1 week on a 3.5-cm diameter rod. The initial rod speed was 4 rpm and with acceleration every 30 s. The time it took for the animal to fall off was recorded. Mice were trained by performing three trials on each of 3 consecutive days prior to testing. Mice were placed on the rod, and the speed was gradually increased from 4 to 40 rotations per minute (rpm). The trial lasted until the mouse fell from the rod or until the mouse remained on the rod for 600 s. Testing was performed on the fourth day using two different speeds, 20 and 32 rpm. The latency to fall was calculated for each speed.

Grip strength test

We focused only on hindlimb strength based on our treatment level. Mice were held by the neck skin and lowered toward the apparatus (Ugo Basile) until they grabbed a grid with both hindlimbs. Mice were gently pulled forward until they released their grip from the grid. Each session consisted of five consecutive trials. The equipment automatically measures the grams of force required to pry the mouse from the grid.

Electrophysiological evaluation

Bilateral sciatic nerves were stimulated in anesthetized animals (n = 10 per treatment group) at the sciatic notch and distally at the knee via bipolar electrodes with supramaximal square-wave pulses (5 V) of 0.05 ms. The latencies of CMAPs were recorded by a bipolar electrode inserted between digits 2 and 3 of the hind paw and latencies were measured from the stimulus artifact to the onset of the negative M wave deflection. MNCVs were calculated by dividing the distance between the stimulating and recording electrodes by the result of subtracting the distal latency from the proximal latency.

Evaluation of nodal pathology

To examine whether the characteristic nodal widening that occurs in *Sh3tc2*$^{-/-}$ mice can be rescued by the gene therapy, sciatic nerve teased fibers from WT (n = 3) as well as from full vector-injected (n = 10) and mock vector-injected *Sh3tc2*$^{-/-}$ mice (n = 10) from each treatment time point were examined. Nodal length was assessed by directly measuring the width of Nav1.6 immunoreactive area using ImageJ software. A total of 50 nodes from each animal were measured and average values per animal compared.

Morphometric analysis of myelination

For quantitative analysis of myelination, we obtained toluidine blue-stained transverse semithin sections (1 μm) of PNS tissues following perfusion with 2.5% glutaraldehyde and resin embedding, as

described previously.[18,30,36] We calculated the g-ratios for all myelinated fibers in all treatment groups using Image-Pro software and a custom-made macro, which detects the axons and their myelin sheath according to color. This macro calculates g-ratio by dividing the average inner perimeter of the axon by the average outer perimeter of the axon, as well as the average myelin thickness for each myelinated fiber. Because more pronounced myelination deficits were observed in fibers >4 μm in diameter in the original characterization of this model,[13] we also analyzed the subset of fibers >4 μm in diameter separately along with the analysis of all fibers >1 μm, as described previously.[18] In addition, completely demyelinated fibers (defined as axons >1 μm in diameter devoid of myelin sheath) in anterior lumbar roots and mid-sciatic nerves were manually counted and compared with the total fiber numbers to obtain the ratio of demyelinated fibers.

Measurement of NF-L concentration

Blood samples were collected retro-orbitally from the mice groups subsequently used for morphometric analysis. Blood samples were processed within 1 h. Blood was collected into EDTA-containing tubes and centrifuged at 20°C at 3,500 rpm for 10 min. Plasma was aliquoted and stored at −80°C until testing. Plasma NF-L concentration was measured at University College London (UCL) using a commercially available NF-Light kit on a single molecule array (Simoa) HD-1 instrument (Quanterix, Billerica, MA).[63,64]

Statistical analysis

The percentage of EGFP or SH3TC2-positive Schwann cells in immunostained lumbar roots and sciatic nerves of WT and *Sh3tc2*$^{-/-}$ mice injected with the mock or full vector, respectively, were compared with Student's t test. Behavioral testing results, electrophysiological results, NF-L levels, and morphological analysis data including nodal length obtained from mock and fully treated groups and WT controls were compared by one-way ANOVA with Tukey's multiple-comparison test (significance level for all comparisons, $p < 0.05$). Each set of data is presented as the mean ± SEM. All statistical analyses were performed using GraphPad Prism, version 6 (GraphPad Software).

DATA AND CODE AVAILABILITY

All the data are present in the manuscript or in the supplemental figures.

SUPPLEMENTAL INFORMATION

Supplemental information can be found online at https://doi.org/10.1016/j.ymthe.2023.08.020.

ACKNOWLEDGMENTS

This research was funded by the Charcot-Marie-Tooth Association (CMTA grant 2019-21 to K.A.K.). The NF-L measurements were funded by the UK Dementia Research Institute at UCL (UKDRI-1003 to A.H. and H.Z.).

AUTHOR CONTRIBUTIONS

E.G. performed the experiments, acquired the data, analyzed the data, and wrote the manuscript. A.K. performed electrophysiology experiments. M.S. performed additional evaluations of control animal groups. I.S. conducted cloning and mice PCR screening. N.S. performed and analyzed the reporter gene expression analysis. J.R., C.T., and C.C. performed and analyzed VGCNs. A.H. and H.Z. analyzed plasma NF-L levels. K.A.K. designed research studies and wrote the manuscript. All authors critically reviewed and approved the final manuscript.

DECLARATION OF INTERESTS

The study is part of a WO 2020/245169 A1 application in which A.K., I.S., N.S., and K.A.K. are co-inventors. H.Z. has served at scientific advisory boards and/or as a consultant for Abbvie, Acumen, Alector, Alzinova, ALZPath, Annexon, Apellis, Artery Therapeutics, AZTherapies, CogRx, Denali, Eisai, Nervgen, Novo Nordisk, Optoceutics, Passage Bio, Pinteon Therapeutics, Prothena, Red Abbey Labs, reMYND, Roche, Samumed, Siemens Healthineers, Triplet Therapeutics, and Wave, has given lectures in symposia sponsored by Cellectricon, Fujirebio, Alzecure, Biogen, and Roche, and is a co-founder of Brain Biomarker Solutions in Gothenburg AB (BBS), which is a part of the GU Ventures Incubator Program (outside submitted work).

REFERENCES

1. Azzedine, H., and Salih, M.A. (1993). SH3TC2-Related Hereditary Motor and Sensory Neuropathy. In GeneReviews, M.P. Adam, D.B. Everman, and G.M. Mirzaa, et al., eds. *(R))*.

2. Fridman, V., Bundy, B., Reilly, M.M., Pareyson, D., Bacon, C., Burns, J., Day, J., Feely, S., Finkel, R.S., Grider, T., et al. (2015). CMT subtypes and disease burden in patients enrolled in the Inherited Neuropathies Consortium natural history study: a cross-sectional analysis. J. Neurol. Neurosurg. Psychiatry *86*, 873–878. https://doi.org/10.1136/jnnp-2014-308826.

3. Piscosquito, G., Saveri, P., Magri, S., Ciano, C., Gandioli, C., Morbin, M., Bella, D.D., Moroni, I., Taroni, F., and Pareyson, D. (2016). Screening for SH3TC2 gene mutations in a series of demyelinating recessive Charcot-Marie-Tooth disease (CMT4). J. Peripher. Nerv. Syst. *21*, 142–149. https://doi.org/10.1111/jns.12175.

4. Dohrn, M.F., Glöckle, N., Mulahasanovic, L., Heller, C., Mohr, J., Bauer, C., Riesch, E., Becker, A., Battke, F., Hörtnagel, K., et al. (2017). Frequent genes in rare diseases: panel-based next generation sequencing to disclose causal mutations in hereditary neuropathies. J. Neurochem. *143*, 507–522. https://doi.org/10.1111/jnc.14217.

5. Kessali, M., Zemmouri, R., Guilbot, A., Maisonobe, T., Brice, A., LeGuern, E., and Grid, D. (1997). A clinical, electrophysiologic, neuropathologic, and genetic study of two large Algerian families with an autosomal recessive demyelinating form of Charcot-Marie-Tooth disease. *Neurol.* Apr *48*, 867–873. https://doi.org/10.1212/wnl.48.4.867.

6. Gabreëls-Festen, A., van Beersum, S., Eshuis, L., LeGuern, E., Gabreëls, F., van Engelen, B., and Mariman, E. (1999). Study on the gene and phenotypic characterisation of autosomal recessive demyelinating motor and sensory neuropathy (Charcot-Marie-Tooth disease) with a gene locus on chromosome 5q23-q33. J. Neurol. Neurosurg. Psychiatry *66*, 569–574. https://doi.org/10.1136/jnnp.66.5.569.

7. Azzedine, H., Ravisé, N., Verny, C., Gabrëels-Festen, A., Lammens, M., Grid, D., Vallat, J.M., Durosier, G., Senderek, J., Nouioua, S., et al. (2006). Spine deformities in Charcot-Marie-Tooth 4C caused by SH3TC2 gene mutations. Neurology *67*, 602–606. https://doi.org/10.1212/01.wnl.0000230225.19797.93.

8. Kontogeorgiou, Z., Nikolaou, K., Kartanou, C., Breza, M., Panas, M., Karadima, G., and Koutsis, G. (2019). Mutational screening of the SH3TC2 gene in Greek patients with suspected demyelinating recessive Charcot-Marie-Tooth disease reveals a varied and unusual phenotypic spectrum. J. Peripher. Nerv. Syst. *24*, 125–130. https://doi.org/10.1111/jns.12305.

9. Gooding, R., Colomer, J., King, R., Angelicheva, D., Marns, L., Parman, Y., Chandler, D., Bertranpetit, J., and Kalaydjieva, L. (2005). A novel Gypsy founder mutation, p.Arg1109X in the CMT4C gene, causes variable peripheral neuropathy phenotypes. J. Med. Genet. *42*, e69. https://doi.org/10.1136/jmg.2005.034132.

10. Colomer, J., Gooding, R., Angelicheva, D., King, R.H.M., Guillén-Navarro, E., Parman, Y., Nascimento, A., Conill, J., and Kalaydjieva, L. (2006). Clinical spectrum of CMT4C disease in patients homozygous for the p.Arg1109X mutation in SH3TC2. Neuromuscul. Disord. *16*, 449–453. https://doi.org/10.1016/j.nmd.2006.05.005.

11. Varley, T.L., Bourque, P.R., and Baker, S.K. (2015). Phenotypic variability of CMT4C in a French-Canadian kindred. Muscle Nerve *52*, 444–449. https://doi.org/10.1002/mus.24640.

12. Senderek, J., Bergmann, C., Stendel, C., Kirfel, J., Verpoorten, N., De Jonghe, P., Timmerman, V., Chrast, R., Verheijen, M.H.G., Lemke, G., et al. (2003). Mutations in a gene encoding a novel SH3/TPR domain protein cause autosomal recessive Charcot-Marie-Tooth type 4C neuropathy. Am. J. Hum. Genet. *73*, 1106–1119. https://doi.org/10.1086/379525.

13. Arnaud, E., Zenker, J., de Preux Charles, A.S., Stendel, C., Roos, A., Médard, J.J., Tricaud, N., Kleine, H., Luscher, B., Weis, J., et al. (Oct 13 2009). SH3TC2/KIAA1985 protein is required for proper myelination and the integrity of the node of Ranvier in the peripheral nervous system. Proc. Natl. Acad. Sci. USA *106*, 17528–17533. https://doi.org/10.1073/pnas.0905523106.

14. Laššuthová, P., Mazanec, R., Vondráček, P., Sišková, D., Haberlová, J., Sabová, J., and Seeman, P. (2011). High frequency of SH3TC2 mutations in Czech HMSN I patients. Clin. Genet. *80*, 334–345. https://doi.org/10.1111/j.1399-0004.2011.01640.x.

15. Lupo, V., Galindo, M.I., Martínez-Rubio, D., Sevilla, T., Vílchez, J.J., Palau, F., and Espinós, C. (2009). Missense mutations in the SH3TC2 protein causing Charcot-Marie-Tooth disease type 4C affect its localization in the plasma membrane and endocytic pathway. Hum. Mol. Genet. *18*, 4603–4614. https://doi.org/10.1093/hmg/ddp427.

16. Gouttenoire, E.A., Lupo, V., Calpena, E., Bartesaghi, L., Schüpfer, F., Médard, J.J., Maurer, F., Beckmann, J.S., Senderek, J., Palau, F., et al. (2013). Sh3tc2 deficiency affects neuregulin-1/ErbB signaling. Glia *61*, 1041–1051. https://doi.org/10.1002/glia.22493.

17. Zoupi, L., Savvaki, M., and Karagogeos, D. (2011). Axons and myelinating glia: An intimate contact. IUBMB Life *63*, 730–735. https://doi.org/10.1002/iub.513.

18. Schiza, N., Georgiou, E., Kagiava, A., Médard, J.J., Richter, J., Tryfonos, C., Sargiannidou, I., Heslegrave, A.J., Rossor, A.M., Zetterberg, H., et al. (2019). Gene replacement therapy in a model of Charcot-Marie-Tooth 4C neuropathy. Brain. *142*, 1227–1241. https://doi.org/10.1093/brain/awz064.

19. Foust, K.D., Nurre, E., Montgomery, C.L., Hernandez, A., Chan, C.M., and Kaspar, B.K. (2009). Intravascular AAV9 preferentially targets neonatal neurons and adult astrocytes. Nat. Biotechnol. *27*, 59–65. https://doi.org/10.1038/nbt.1515.

20. Tanguy, Y., Biferi, M.G., Besse, A., Astord, S., Cohen-Tannoudji, M., Marais, T., and Barkats, M. (2015). Systemic AAVrh10 provides higher transgene expression than AAV9 in the brain and the spinal cord of neonatal mice. Front. Mol. Neurosci. *8*, 36. https://doi.org/10.3389/fnmol.2015.00036.

21. Gurda, B.L., De Guilhem De Lataillade, A., Bell, P., Zhu, Y., Yu, H., Wang, P., Bagel, J., Vite, C.H., Sikora, T., Hinderer, C., et al. (2016). Evaluation of AAV-mediated Gene Therapy for Central Nervous System Disease in Canine Mucopolysaccharidosis VII. Mol. Ther. *24*, 206–216. https://doi.org/10.1038/mt.2015.189.

22. Kagiava, A., Karaiskos, C., Richter, J., Tryfonos, C., Jennings, M.J., Heslegrave, A.J., Sargiannidou, I., Stavrou, M., Zetterberg, H., Reilly, M.M., et al. (2021). AAV9-mediated Schwann cell-targeted gene therapy rescues a model of demyelinating neuropathy. Gene Ther. *28*, 659–675. https://doi.org/10.1038/s41434-021-00250-0.

23. Bradbury, A.M., Rafi, M.A., Bagel, J.H., Brisson, B.K., Marshall, M.S., Pesayco Salvador, J., Jiang, X., Swain, G.P., Prociuk, M.L., ODonnell, P.A., et al. (2018). AAVrh10 Gene Therapy Ameliorates Central and Peripheral Nervous System Disease in Canine Globoid Cell Leukodystrophy (Krabbe Disease). Hum. Gene Ther. *29*, 785–801. https://doi.org/10.1089/hum.2017.151.

24. Calcedo, R., and Wilson, J.M. (2013). Humoral Immune Response to AAV. Front. Immunol. *4*, 341. https://doi.org/10.3389/fimmu.2013.00341.

25. Hargrove, P.W., Kepes, S., Hanawa, H., Obenauer, J.C., Pei, D., Cheng, C., Gray, J.T., Neale, G., and Persons, D.A. (2008). Globin lentiviral vector insertions can perturb the expression of endogenous genes in beta-thalassemic hematopoietic cells. Mol. Ther. *16*, 525–533. https://doi.org/10.1038/sj.mt.6300394.

26. Day, J.W., Mendell, J.R., Mercuri, E., Finkel, R.S., Strauss, K.A., Kleyn, A., Tauscher-Wisniewski, S., Tukov, F.F., Reyna, S.P., and Chand, D.H. (2021). Clinical Trial and Postmarketing Safety of Onasemnogene Abeparvovec Therapy. Drug Saf. *44*, 1109–1119. https://doi.org/10.1007/s40264-021-01107-6.

27. Mercuri, E., Muntoni, F., Baranello, G., Masson, R., Boespflug-Tanguy, O., Bruno, C., Corti, S., Daron, A., Deconinck, N., Servais, L., et al. (2021). Onasemnogene abeparvovec gene therapy for symptomatic infantile-onset spinal muscular atrophy type 1 (STR1VE-EU): an open-label, single-arm, multicentre, phase 3 trial. Lancet Neurol. *20*, 832–841. https://doi.org/10.1016/S1474-4422(21)00251-9.

28. Stavrou, M., Kagiava, A., Choudury, S.G., Jennings, M.J., Wallace, L.M., Fowler, A.M., Heslegrave, A., Richter, J., Tryfonos, C., Christodoulou, C., et al. (2022). A translatable RNAi-driven gene therapy silences PMP22/Pmp22 genes and improves neuropathy in CMT1A mice. J. Clin. Invest. *132*, e159814. https://doi.org/10.1172/JCI159814.

29. Scherer, S.S., Xu, Y.T., Messing, A., Willecke, K., Fischbeck, K.H., and Jeng, L.J.B. (2005). Transgenic expression of human connexin32 in myelinating Schwann cells prevents demyelination in connexin32-null mice. J. Neurosci. *25*, 1550–1559. https://doi.org/10.1523/JNEUROSCI.3082-04.2005.

30. Sargiannidou, I., Kagiava, A., Bashiardes, S., Richter, J., Christodoulou, C., Scherer, S.S., and Kleopa, K.A. (2015). Intraneural GJB1 gene delivery improves nerve pathology in a model of X-linked Charcot-Marie-Tooth disease. Ann. Neurol. *78*, 303–316. https://doi.org/10.1002/ana.24441.

31. Jang, S.W., and Svaren, J. (2009). Induction of myelin protein zero by early growth response 2 through upstream and intragenic elements. J. Biol. Chem. *284*, 20111–20120. https://doi.org/10.1074/jbc.M109.022426.

32. Kagiava, A., Richter, J., Tryfonos, C., Leal-Julià, M., Sargiannidou, I., Christodoulou, C., Bosch, A., and Kleopa, K.A. (2021). Efficacy of AAV serotypes to target Schwann cells after intrathecal and intravenous delivery. Sci. Rep. *11*, 23358. https://doi.org/10.1038/s41598-021-02694-1.

33. Greenshpan, Y., Sharabi, O., Yegodayev, K.M., Novoplansky, O., Elkabets, M., Gazit, R., and Porgador, A. (2022). The Contribution of the Minimal Promoter Element to the Activity of Synthetic Promoters Mediating CAR Expression in the Tumor Microenvironment. Int. J. Mol. Sci. *23*, 7431. https://doi.org/10.3390/ijms23137431.

34. Kügler, S., Lingor, P., Schöll, U., Zolotukhin, S., and Bähr, M. (2003). Differential transgene expression in brain cells in vivo and in vitro from AAV-2 vectors with small transcriptional control units. Virology *311*, 89–95. https://doi.org/10.1016/s0042-6822(03)00162-4.

35. Shevtsova, Z., Malik, J.M.I., Michel, U., Bähr, M., and Kügler, S. (2005). Promoters and serotypes: targeting of adeno-associated virus vectors for gene transfer in the rat central nervous system in vitro and in vivo. Exp. Physiol. *90*, 53–59. https://doi.org/10.1113/expphysiol.2004.028159.

36. Kagiava, A., Sargiannidou, I., Theophilidis, G., Karaiskos, C., Richter, J., Bashiardes, S., Schiza, N., Nearchou, M., Christodoulou, C., Scherer, S.S., and Kleopa, K.A. (2016). Intrathecal gene therapy rescues a model of demyelinating peripheral neuropathy. Proc. Natl. Acad. Sci. USA *113*, E2421–E2429. https://doi.org/10.1073/pnas.1522202113.

37. Choi, S.H., Kim, Y.H., Hebisch, M., Sliwinski, C., Lee, S., D'Avanzo, C., Chen, H., Hooli, B., Asselin, C., Muffat, J., et al. (2014). A three-dimensional human neural cell culture model of Alzheimer's disease. Nature *515*, 274–278. https://doi.org/10.1038/nature13800.

38. Georgiou, E., Sidiropoulou, K., Richter, J., Papaneophytou, C., Sargiannidou, I., Kagiava, A., von Jonquieres, G., Christodoulou, C., Klugmann, M., and Kleopa, K.A. (2017). Gene therapy targeting oligodendrocytes provides therapeutic benefit in a leukodystrophy model. Brain. *140*, 599–616. https://doi.org/10.1093/brain/aww351.

39. Pattali, R., Mou, Y., and Li, X.J. (2019). AAV9 Vector: a Novel modality in gene therapy for spinal muscular atrophy. Gene Ther. *26*, 287–295. https://doi.org/10.1038/s41434-019-0085-4.

40. Naso, M.F., Tomkowicz, B., Perry, W.L., 3rd, and Strohl, W.R. (2017). Adeno-Associated Virus (AAV) as a Vector for Gene Therapy. BioDrugs. *31*, 317–334. https://doi.org/10.1007/s40259-017-0234-5.

41. Kuzmin, D.A., Shutova, M.V., Johnston, N.R., Smith, O.P., Fedorin, V.V., Kukushkin, Y.S., van der Loo, J.C.M., and Johnstone, E.C. (2021). The clinical landscape for AAV gene therapies. Nat. Rev. Drug Discov. *20*, 173–174. https://doi.org/10.1038/d41573-021-00017-7.

42. Glascock, J.J., Shababi, M., Wetz, M.J., Krogman, M.M., and Lorson, C.L. (2012). Direct central nervous system delivery provides enhanced protection following vector mediated gene replacement in a severe model of spinal muscular atrophy. Biochem. Biophys. Res. Commun. *417*, 376–381. https://doi.org/10.1016/j.bbrc.2011.11.121.

43. Rafi, M.A., Rao, H.Z., Luzi, P., Curtis, M.T., and Wenger, D.A. (2012). Extended normal life after AAVrh10-mediated gene therapy in the mouse model of Krabbe disease. Mol. Ther. *20*, 2031–2042. https://doi.org/10.1038/mt.2012.153.

44. Bravo-Hernandez, M., Tadokoro, T., Navarro, M.R., Platoshyn, O., Kobayashi, Y., Marsala, S., Miyanohara, A., Juhas, S., Juhasova, J., Skalnikova, H., et al. (2020). Spinal subpial delivery of AAV9 enables widespread gene silencing and blocks motoneuron degeneration in ALS. Nat. Med. *26*, 118–130. https://doi.org/10.1038/s41591-019-0674-1.

45. Duque, S.I., Arnold, W.D., Odermatt, P., Li, X., Porensky, P.N., Schmelzer, L., Meyer, K., Kolb, S.J., Schümperli, D., Kaspar, B.K., and Burghes, A.H.M. (2015). A large animal model of spinal muscular atrophy and correction of phenotype. Ann. Neurol. *77*, 399–414. https://doi.org/10.1002/ana.24332.

46. Foust, K.D., Salazar, D.L., Likhite, S., Ferraiuolo, L., Ditsworth, D., Ilieva, H., Meyer, K., Schmelzer, L., Braun, L., Cleveland, D.W., and Kaspar, B.K. (2013). Therapeutic AAV9-mediated suppression of mutant SOD1 slows disease progression and extends survival in models of inherited ALS. Mol. Ther. *21*, 2148–2159. https://doi.org/10.1038/mt.2013.211.

47. Gessler, D.J., Li, D., Xu, H., Su, Q., Sanmiguel, J., Tuncer, S., Moore, C., King, J., Matalon, R., and Gao, G. (Feb 9 2017). Redirecting N-acetylaspartate metabolism in the central nervous system normalizes myelination and rescues Canavan disease. JCI Insight *2*, e90807. https://doi.org/10.1172/jci.insight.90807.

48. Bevan, A.K., Duque, S., Foust, K.D., Morales, P.R., Braun, L., Schmelzer, L., Chan, C.M., McCrate, M., Chicoine, L.G., Coley, B.D., et al. (2011). Systemic gene delivery in large species for targeting spinal cord, brain, and peripheral tissues for pediatric disorders. Mol. Ther. *19*, 1971–1980. https://doi.org/10.1038/mt.2011.157.

49. Gautier, B., Hajjar, H., Soares, S., Berthelot, J., Deck, M., Abbou, S., Campbell, G., Ceprian, M., Gonzalez, S., Fovet, C.M., et al. (2021). AAV2/9-mediated silencing of PMP22 prevents the development of pathological features in a rat model of Charcot-Marie-Tooth disease 1 A. Nat. Commun. *12*, 2356. https://doi.org/10.1038/s41467-021-22593-3.

50. Kagiava, A., Karaiskos, C., Richter, J., Tryfonos, C., Lapathitis, G., Sargiannidou, I., Christodoulou, C., and Kleopa, K.A. (2018). Intrathecal gene therapy in mouse models expressing CMT1X mutations. Hum. Mol. Genet. *27*, 1460–1473. https://doi.org/10.1093/hmg/ddy056.

51. Arancibia-Carcamo, I.L., Ford, M.C., Cossell, L., Ishida, K., Tohyama, K., and Attwell, D. (2017). Node of Ranvier length as a potential regulator of myelinated axon conduction speed. Elife *6*. https://doi.org/10.7554/eLife.23329.

52. Feinberg, K., Eshed-Eisenbach, Y., Frechter, S., Amor, V., Salomon, D., Sabanay, H., Dupree, J.L., Grumet, M., Brophy, P.J., Shrager, P., and Peles, E. (2010). A glial signal consisting of gliomedin and NrCAM clusters axonal Na+ channels during the formation of nodes of Ranvier. Neuron *65*, 490–502. https://doi.org/10.1016/j.neuron.2010.02.004.

53. Amor, S., Peferoen, L.A.N., Vogel, D.Y.S., Breur, M., van der Valk, P., Baker, D., and van Noort, J.M. (2014). Inflammation in neurodegenerative diseases–an update. Immunology *142*, 151–166. https://doi.org/10.1111/imm.12233.

54. Stendel, C., Roos, A., Kleine, H., Arnaud, E., Ozçelik, M., Sidiropoulos, P.N.M., Zenker, J., Schüpfer, F., Lehmann, U., Sobota, R.M., et al. (2010). SH3TC2, a protein mutant in Charcot-Marie-Tooth neuropathy, links peripheral nerve myelination to endosomal recycling. Brain. *133* (Pt 8), 2462–2474. https://doi.org/10.1093/brain/awq168.

55. Roberts, R.C., Peden, A.A., Buss, F., Bright, N.A., Latouche, M., Reilly, M.M., Kendrick-Jones, J., and Luzio, J.P. (2010). Mistargeting of SH3TC2 away from the recycling endosome causes Charcot-Marie-Tooth disease type 4C. Hum. Mol. Genet. *19*, 1009–1018. https://doi.org/10.1093/hmg/ddp565.

56. Trapp, B.D., Kidd, G.J., Hauer, P., Mulrenin, E., Haney, C.A., and Andrews, S.B. (1995). Polarization of myelinating Schwann cell surface membranes: role of microtubules and the trans-Golgi network. J. Neurosci. *15* (3 Pt 1), 1797–1807. https://doi.org/10.1523/JNEUROSCI.15-03-01797.1995.

57. Kidd, G., Andrews, S.B., and Trapp, B.D. (1996). Axons regulate the distribution of Schwann cell microtubules. J. Neurosci. *16*, 946–954. https://doi.org/10.1523/JNEUROSCI.16-03-00946.1996.

58. Kreitzer, G., Schmoranzer, J., Low, S.H., Li, X., Gan, Y., Weimbs, T., Simon, S.M., and Rodriguez-Boulan, E. (2003). Three-dimensional analysis of post-Golgi carrier exocytosis in epithelial cells. Nat. Cell Biol. *5*, 126–136. https://doi.org/10.1038/ncb917.

59. Cipriani, S., Phan, V., Médard, J.J., Horvath, R., Lochmüller, H., Chrast, R., Roos, A., and Spendiff, S. (2018). Neuromuscular Junction Changes in a Mouse Model of Charcot-Marie-Tooth Disease Type 4C. Int. J. Mol. Sci. *19*, 4072. https://doi.org/10.3390/ijms19124072.

60. Rossor, A.M., Kapoor, M., Wellington, H., Spaulding, E., Sleigh, J.N., Burgess, R.W., Laura, M., Zetterberg, H., Bacha, A., Wu, X., et al. (2022). A longitudinal and cross-sectional study of plasma neurofilament light chain concentration in Charcot-Marie-Tooth disease. J. Peripher. Nerv. Syst. *27*, 50–57. https://doi.org/10.1111/jns.12477.

61. Geraerts, M., Willems, S., Baekelandt, V., Debyser, Z., and Gijsbers, R. (2006). Comparison of lentiviral vector titration methods. BMC Biotechnol. *6*, 34. https://doi.org/10.1186/1472-6750-6-34.

62. Kagiava, A., and Kleopa, K.A. (2018). Intrathecal Delivery of Viral Vectors for Gene Therapy. Methods Mol. Biol. *1791*, 277–285. https://doi.org/10.1007/978-1-4939-7862-5_22.

63. Sandelius, Å., Zetterberg, H., Blennow, K., Adiutori, R., Malaspina, A., Laura, M., Reilly, M.M., and Rossor, A.M. (2018). Plasma neurofilament light chain concentration in the inherited peripheral neuropathies. *Neurol.* Feb 6 *90*, e518–e524. https://doi.org/10.1212/WNL.0000000000004932.

64. Rohrer, J.D., Woollacott, I.O.C., Dick, K.M., Brotherhood, E., Gordon, E., Fellows, A., Toombs, J., Druyeh, R., Cardoso, M.J., Ourselin, S., et al. (2016). Serum neurofilament light chain protein is a measure of disease intensity in frontotemporal dementia. Neurology *87*, 1329–1336. https://doi.org/10.1212/WNL.0000000000003154.